

Deep particle stocks following the summer bloom around the Kerguelen islands: Insights into diatoms physiological state, community structure and mortality modes

Leblanc Karine ^{1,*}, Lafond Augustin ¹, Cornet Veronique ¹, Legras Justine ¹, Marie Barbara ²,
Queguiner Bernard ¹

¹ Aix Marseille Univ., Université de Toulon, CNRS, IRD, MIO UM 110, 13288 Marseille, France

² Sorbonne Université, CNRS, Laboratoire d'Océanographie Microbienne, LOMIC, F-66650 Banyuls/mer, France

* Corresponding author : Karine Leblanc, email address : karine.leblanc@univ-amu.fr

Abstract :

Particles located at the interface between the surface ocean layer and the top of the mesopelagic domain are the initial vector of the biological pump yet, their nature is still largely unknown. During the MOBYDICK cruise in the vicinity of the Kerguelen Islands (Indian sector of the Southern Ocean) we deployed a recently available device that concentrates and collects deep particles over a predetermined layer of water. In this paper, we present a detailed description of the collected particles and individual planktonic cells, including their taxonomy, carbon and lipid content, as well as cell viability, in order to characterize the particle stocks present at depth. The cruise was carried out at the end of the summer bloom, a period characterized by declining stocks of biogenic material associated with various mortality processes of planktonic organisms. Unexpectedly, the majority of the collected particles consisted of single empty diatom frustules, while fecal pellets and aggregates accounted for only a minor fraction. Distinct mortality processes, from parasitic infection to mesozooplankton grazing, and distinct silicification degrees as well as different life stages could be identified in relation to diatom taxa suggesting the occurrence of several export modes to intermediate and deep layers within the diatom community. We observed a dominant contribution of single cell diatoms ($93 \pm 6\%$) to the deep particle stocks but a very small contribution of intact diatom cells ($\sim 0.3\%$) to C content in the intermediate layer (125–500 m), together with a very small fecal pellet contribution, that was dominated by the minipellet size-class. Taxonomical analyses revealed distinct communities west of Kerguelen in the HNLC area compared to the island's fertilized plateau and its eastern flank. Differences in silicification degrees as well as distinct mortality/export processes linked to surface nutrient depletion and trophic interactions (such as parasitic infection or grazing by phaeodarians) were identified in the upper layer, leading to distinct contributions of major diatom taxa to deep suspended particles.

Highlights

► There is a dominant contribution of single cell diatoms to the deep particle stocks. ► There is a very small fecal pellet contribution at depth by the end of summer, dominated by minipellets. ► Distinct mortality/export processes in the upper layer control the contribution of major diatom taxa to deep suspended particles.

Keywords : Biological carbon pump, Diatoms, Mortality modes, Southern Ocean, Diversity, Deep particle stocks

1. Introduction

The global carbon (C) export to the deep ocean is still poorly constrained and estimates range from 5 to 20 Pg C yr⁻¹ (Laws et al., 2000; Henson et al., 2011; Puigcorb  et al., 2020). Despite the overarching importance of this process in Earth climate regulation, the mechanisms responsible for the variability of carbon export are still largely unknown. Characterizing the composition of the particulate C flux to depth together with the intricate ecological processes that can alter particle sinking rates are crucial in this context. Until now, the focus has been placed mainly on large (>500 µm) aggregates and fecal pellets, otherwise known as marine snow, as primary vectors of C to the ocean's interior, mainly because of their elevated sinking rates, ranging from 5 to 2,700 m d⁻¹ (Turner, 2002; Riley et al., 2012). Methodological challenges to accurately quantify the flux of diverse types of particles over the entire size spectrum, from µm to mm, have been identified already in the 80s (Alldredge and Silver, 1988) but are still difficult to overcome today, as no single instrument is able to characterize and quantify the entire particle size range together with its species-specific composition (Durkin et al., 2015). Recently, it has been suggested that *in-situ* aggregate size is not a sufficient descriptor for inferring their sinking rates and that more information is needed on their excess density, age, composition and porosity (Iversen and Lampitt, 2020, Laurenceau-Cornec et al., 2020).

Furthermore, the taxonomic composition of phytoplankton, their biomineral content, and the physiological status of cells in the surface layer have been recognized as central in marine snow genesis (Alldredge and Gotschalk, 1990; Klaas and Archer, 2002, Laurenceau-Cornec et al., 2019). Until recently, the importance of single cells, and in particular small phytoplankton (Waite et al., 2000; Richardson and Jackson, 2007), was not recognized because their sinking rate was deemed too slow to lead to any significant contribution to C export. Yet, recent studies report the presence of small particles under the form of single cells down to 1,000 m and deeper (Di Tullio et al., 2000; Dall'Olmo and Mork, 2014; Agusti et al., 2015, 2020; Durkin et al., 2016; Leblanc et al., 2018) revealing a potential important contribution of single cells to deep C stocks. The mechanisms invoked to explain these new observations are usually aggregation/disaggregation processes during descent in the water column, or entrainment through the mixed layer pump, in which deep mixing brings surface cells

to depth rapidly, but such processes have not been clearly demonstrated so far (Gardner et al., 1995; Stemmann et al., 2004; Richardson and Jackson, 2007; Close et al., 2013; Giering et al., 2014; Durkin et al., 2015; Leblanc et al., 2018). A recent study carried out in the North Atlantic however estimated that eddy driven subduction could contribute to as much as 50% of total POC export (Omand et al., 2015). Only a few studies have hitherto reported the importance of whole diatom cells and spores in sinking C flux (Kemp et al., 2000; Riaux-Gobin et al., 2006; Salter et al., 2007; Rembauville et al., 2015; Romero and Fischer, 2017) but the exact quantitative contribution of single cells to deep C stocks and fluxes remains unknown (Le Moigne, 2019) as direct C measurements associated to intact phytoplankton cells are time consuming and seldom undertaken (Assmy et al., 2013; Rembauville et al., 2015). It remains unclear whether this deep C stock in the form of small individual cells plays a role in increasing the particulate C flux either directly or through deep aggregation and/or repackaging processes (Lam and Marchal, 2015).

Similarly, fecal pellets are commonly examined in the large size fraction (at least > 50 μm) but the role of minipellets (3-50 μm) initially described by Gowing and Silver, (1985) has been overlooked. Minipellets can be produced by many different heterotrophs but are often linked to Phaeodaria, a group of siliceous Rhizaria (Gonzalez, 1992). Minipellets have been shown to represent a flux equivalent to 11-49% of the C flux of larger fecal pellets in the Eastern Tropical Pacific Ocean (Gowing and Silver, 1985). This size-class of fecal pellets has been reported as extremely abundant in a series of field studies from the late 80s and early 90s conducted in the Eastern Tropical (Gowing and Silver, 1985) and North Pacific (Gowing, 1986), in the Atlantic (Riemann, 1989) as well as in the Southern Ocean along the Antarctic peninsula (Gonzalez, 1992). These types of particles have been ignored for more than 30 years in most biological C pump studies, except for a temporal survey from the Northeast Atlantic, where high summer POC fluxes at 3000 m were shown to follow peaks in phaeodarian abundance (Lampitt et al., 2009). Recently, a renewed interest emerged with the recognized importance of Phaeodaria's role on both the Si and C cycle in the mesopelagic zone in the world ocean (Stukel et al., 2018; Biard et al., 2018). Another recent study in the North Pacific estimated that this group accounted for up to 10% of the total organic carbon of sinking particles (Ikenoue et al., 2019). Hence, marine snow and particles in the small size-range (<50-100 μm) have until recently not been in the spotlight, for obvious methodological issues, and their relative contribution to deep C stocks and fluxes remains to be fully quantified in various oceanic regimes.

In 2015, a new device, called the Bottle net (Aquatic BioTechnology™) has allowed for methodological improvements in the collection of deep particle stocks. The device enables a rapid, detailed sampling of depth-integrated concentrated material collected over a very short time period (during a CTD upcast), allowing for taxonomical but also for physiological rate measurements since collection time is equal to that of Niskin samples (Agusti et al., 2015). Collection of particles between 2,000 and 4,000 m with this device during the Malaspina circumnavigation program in the subtropical oligotrophic ocean revealed the ubiquitous presence of fresh single cells in this deep layer. Diatoms, which do not dominate in surface oligotrophic waters, were surprisingly major contributors to microplankton cells at depth (81.5%)

and a large proportion (18%) were intact viable cells, implying fast sinking rates estimated to 124-732 m d⁻¹ (Agusti et al., 2015) comparable to aggregates and fecal pellet sinking rates. The Bottle net allows for a detailed analysis of small microplankton (>20 µm) cells and particles in microscopy, while sediment traps designed to measure downward fluxes do not adequately sample this small fraction, which is often merged in larger aggregates and phytodetritus within the collection cups and for which individual C content quantification is difficult. It is complementary to polyacrylamide gel-filled traps which also allow to study the contribution of individual cells and chains to the particulate flux (Laurenceau-Cornec et al., 2015).

A Bottle net was deployed during the MOBYDICK (Marine Ecosystem Biodiversity and Dynamics of Carbon around Kerguelen: an integrated view) cruise in the vicinity of the Kerguelen Islands in February-March 2018, a period coinciding with the demise of the recurrent summer bloom. The study region is considered as a natural fertilization laboratory (Blain et al., 2008), and several previous studies focused on the large phytoplankton bloom resulting from the island's Fe-enrichment of the plateau area by comparison to the neighboring HNLC (High Nutrient Low Chlorophyll) region (Cornet-Barthaux et al., 2007; Mosseri et al., 2008; Armand et al., 2008a; Quéguiner, 2013; Lasbleiz et al., 2014; Lasbleiz et al., 2016). In this study, we aimed to investigate the nature of the deep particles using the Bottle-net and compare their composition with surface communities collected with Phytonets and complementary details of the surface diatom communities from CTD Niskin collection (Lafond et al., 2020). We aimed at identifying preferential modes of export of surface particles and single cells, and investigate potential trophic relationships or life strategies such as spore formation, which could impact the efficiency of the biological pump.

2. Material and methods

2.1. Study site

The MOBYDICK cruise took place between February 18th and March 27th, 2018 aboard the R/V Marion Dufresne south of the Kerguelen Islands (Southern Ocean). Four stations were investigated with repeated visits (Fig. 1, Table 1), including two so-called reference stations, M2 (sampled thrice) and M4 (sampled twice), corresponding respectively to the Fe-enriched plateau and the HNLC off-plateau area. To increase information on the spatial variability, two intermediate stations, M1 and M3 were additionally sampled, once and twice respectively. Bottom depths spanned from 520 m at M2 to 4,730 m at M4. According to Pauthenet et al. (2018), station M3 was located within the Polar Frontal zone at this time of the year, whereas the other stations were located in the POOZ (Permanently Open Ocean Zone) of the Antarctic zone, with M1 and M4 both situated very close to the Polar Front (Fig. 1).

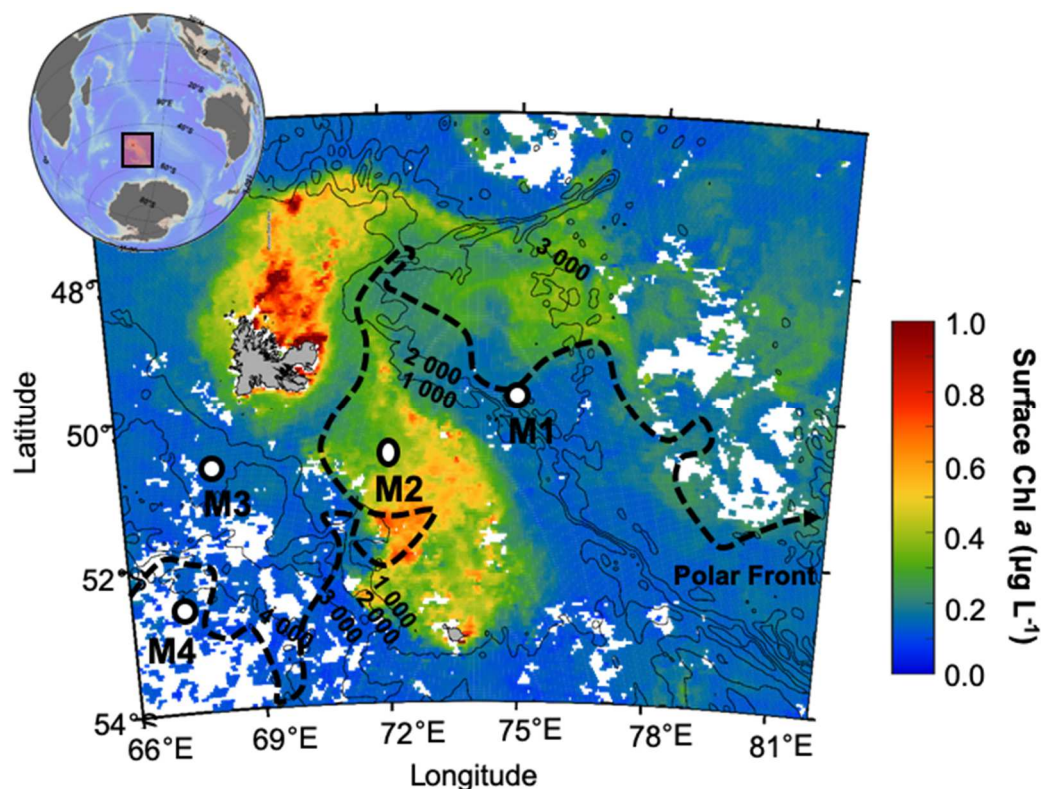


Figure 1: Station map of the four sampling sites around the Kerguelen Plateau, with surimposed satellite-Chl *a* map (MODIS level 3 product) averaged over March 2018). Contour lines represent the bathymetry (m). The dotted line represents the position of the Polar Front (PF) according to Pauthenet et al. (2018)

Table 1: Metadata and hydrographical conditions at stations sampled during the MOBYDICK expedition.

Station	Latitude/Longitude	Date	Bottom depth (m)	MLD (m)	Ze 1% (m)	H ₄ SiO ₄ :NO ₃ ⁻
M1	49.85°S ; 74.90°E	09/03/2018	2 723	63	89	0.27 ± 0.01
M2-1	50.62°S ; 72.00°E	26/02/2018	520	79	64	0.06 ± 0.02
M2-2		06/03/2018		73	61	0.08 ± 0.03
M2-3		16/03/2018		80	58	0.13 ± 0.01
M3-1	50.68°S ; 68.06°E	04/03/2018	1730	74	93	0.12 ± 0.04
M3-3		19/03/2018		96	105	0.20 ± 0.17
M4-1	52.60°S ; 67.20°E	01/03/2018	4 731	69	95	0.17 ± 0.01
M4-2		12/03/2018		96	101	0.22 ± 0.04

2.2. Phytonet sampling

A 35 µm mesh phytoplankton net (hereafter called Phytonet) with a mouth opening of 50 cm diameter was deployed at all sites. Vertical net hauls were consistently realized between 0 and 125 m depth, with an approximate filtered seawater volume of 24 m³. Once on board, the net was gently rinsed from the outside using a hose delivering surface seawater. The window of the plankton collector was rinsed with a squirt bottle filled with 0.2 µm filtered seawater to unclog all aggregates. The entire

remaining volume (between 400-500 mL) was immediately transferred to a polycarbonate bottle, which was then subsampled for diversity and cellular activity.

2.3. Bottle net sampling

A Bottle net (Aquatic Biotechnology™) was mounted on the rosette and deployed at each site. The device is a modified PVC bottle, holding a vertical 20 µm-plankton mesh and a plankton collector, that can be opened and closed between two chosen layers, to collect particles during the upcast (Agusti et al., 2015). Variable sampling depths were covered at each site and revisit depending on bottom bathymetry and CTD-profiles (Table 1, Fig. 2) for a total of 20 Bottle net casts. The intermediate layer (between approximately 125 and 500 m) was sampled at least once at each site, together with deeper layers whenever possible. At station M4-2, two Bottle net casts (125-250 and 250-500 m) were combined for better comparison with the other stations. The Bottle net top opening is round-shaped and similar in size to a standard Niskin bottle (7.5 cm diameter) and the amount of water filtered by the 20 µm mesh varied between 0.1 m³ (for the 125-150 m cast) and 9.5 m³ (for the deep 1900-4000 m cast). Sampling with the CTD was performed at half speed (0.5 m/s) during the Bottle net operations. Given the large body of water filtered, the total amount of particles and cells collected in approximately 50 mL of seawater varied between 26×10^6 and 28×10^7 , thus allowing for a complete diversity analysis on concentrated material compared to Niskin bottles that contain only a very low average particle concentration in deep waters.

Blanks. The design of the Bottle net unfortunately renders the closing lid vulnerable to lifting by the up and down pulling motion during the upcast if the rosette is stopped several times in the surface layer in order to close other Niskin bottles. In order to assess the contamination that might arise from plankton rich surface water seeping into the Bottle net during this stop-and-go ascent period, we carried out 5 blank casts (3 at M2 and 2 at M3), with the Bottle net closed during the entire cast. Blank samples were then counted for particles and compared to the average counts measured at both stations. At M2, the blank samples contained 8.7% of the average cell counts and was mostly comprised of *Corethron inerme* filaments which were accumulating in the surface layer, while at M3, blank casts represented 2.7% of the average cell counts. Despite this slight contamination from surface waters, we are confident that our subsequent analyses and comparison to surface communities allowed to filter out this signal and still give valid conclusions on the nature of deep particles and export-related processes.

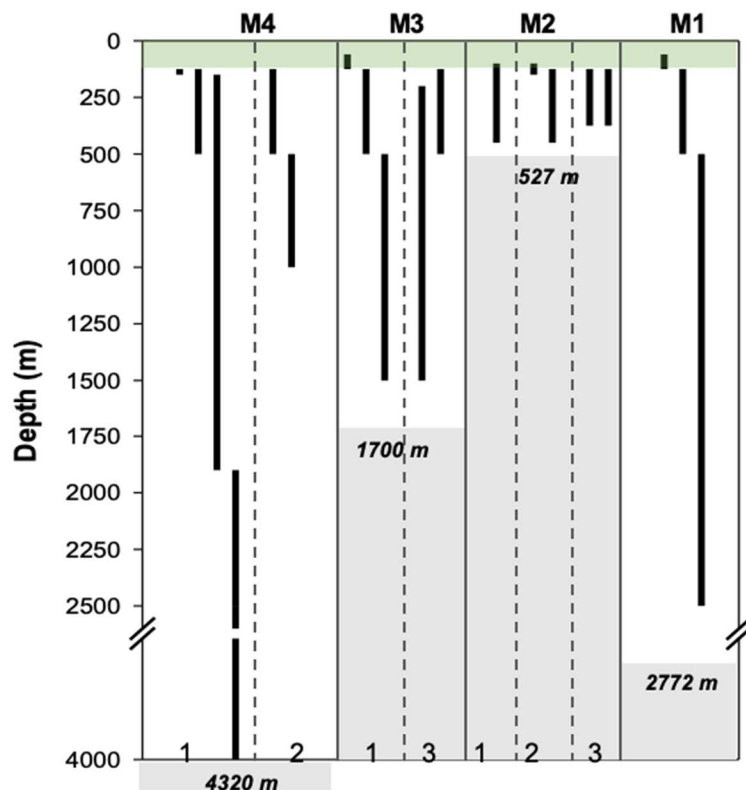


Figure 2: Bottle net casts depths at the 4 different sampling sites from west to east, and for the different revisits (1,2,3). Bottom bathymetry is indicated in bold italic numbers. The green rectangle indicates the phytonet collection depth in the surface layer from 0 to 125 m.

Collection. Samples were collected from the Bottle net on deck, after careful rinsing of its plankton net with a squirt bottle filled with 0.2 μm filtered seawater. The collected volume varied between 48 and 70 mL of seawater. Each sample was transferred immediately into a polypropylene vial and very gently homogenized before several aliquots were subsampled for biogenic silica (BSi), microscopical identification, diatom viability and lipid content.

2.4. Microscopical analyses

2.4.1. Taxonomical identification and counting on Phytonet and Bottle net samples. Two samples for diversity were fixed with acidified lugol and pH-buffered formol, while a third sample was filtered onto a 25 mm 0.2 μm polycarbonate filter, rinsed with milliQ water then dried at room temperature, for Scanning Electron Microscopy (SEM) analyses. Upon sample collection from both the Bottle net and the Phytonet, a small aliquot was systematically observed on board within 30 min of collection using a bright-field Nikon TE-200 inverted microscope to observe any trophic behavior or parasitic activity. Further cell counts were later performed in the ground-based laboratory on a Nikon TE-200 inverted microscope, while detailed species identification has been carried out on a Phenom-Pro benchtop scanning electron microscope at 10 kV using the untreated and uncoated dried filters. Species identification relied mostly on Priddle and Fryxell (1985) and Scott and Marchant (2005).

2.4.2. Observation of fecal pellets and aggregates on Phytonet and Bottle net samples.

Different types of particles observed by SEM or bright-field microscopy could be identified as fecal pellets or aggregates. Although precautions were taken in handling the samples to avoid breaking down, it is impossible to accurately assess the effect of subsequent storage on the integrity of these fragile structures. However, direct examination on board immediately after sampling by bottlenets and phytonets and the subsequent quantification step in the laboratory showed no noticeable difference: in both cases, fecal pellets and aggregates represented only a very minor fraction of the collected particles. What could not be assessed was the amount of material disintegrated by the net mesh during collection, but intact fecal pellets and varying degrees of loose, cohesive aggregates were observed later, suggesting overall good preservation.

2.4.3. Mortality processes on Phytonet and Bottle net samples. In order to gain further insights into biological interactions and mortality processes in the diatom community, we carefully identified cell status: intact (e.g. cytoplasm still present and visually unaltered), empty (e.g. completely intact frustule with no cytoplasm visible), broken (e.g. with a clean break at the girdle band junction), crunched (e.g. frustule with a jagged break outside of the girdle junction, suppl. Fig. S1), or infected (e.g. frustule filled with small black cells, suppl. Fig. S2). While many mortality pathways can explain the presence of empty and broken frustules, crunched frustules are most likely due to handling by copepod or amphipod mandibles (Assmy et al., 2007). Life stages such as resting spores and resting cells (mainly of *Odontella weissflogii*), as well as different morphological/winter forms within some species (e.g. *Chaetoceros atlanticus*, *Eucampia antarctica*) were also identified and counted separately (suppl. Fig. S3).

2.4.4. Diatom viability on Phytonet and Bottle net samples. To further improve the physiological description of diatom cells, we used the SYTOX Green viability probe (Veldhuis et al., 2001) on all Phytonets samples and on 13 out of 20 Bottle net samples. Upon collection, 990 μ L of sample was placed in an Eppendorf PE 1.5 ml vial and spiked with 10 μ L of 500 μ L SYTOX Green Nucleic Acid Stain (S7020, Life Technologies™) 5 mM solution, for a final concentration of 5 μ M and gently agitated. Samples were incubated for 30 min in the dark at *in situ* sampling temperature (4°C), then transferred onto a Sedgewick Rafter graduated 1 mL chamber and immediately counted on board on a Zeiss imager A2 epifluorescence microscope, using an FITC filter cube (λ_{ex} : 479/39 nm, λ_{em} : 522/40 nm, 497 nm LP). Non-viable cells, which have lost membrane integrity, incorporate the probe and their nuclei display a green fluorescence, while viable cells with intact membranes only show chlorophyll *a* (Chl *a*) red autofluorescence.

2.4.5. Lipid content on Bottle net samples. The accumulation of intracellular lipids inside diatom cells can be an indication of the presence of resting stages, which often do not show any visible morphological differences with vegetative cells (Kaczmarek et al., 2013 ; Ellegaard and Ribeiro, 2018). Cell lipids in cells, as a way of identifying resting stages and spores, were assessed using Nile Red labelling (Greenspan,

1985). Seawater samples were treated on board immediately after collection. Cells were resuspended in 1 ml HEPES buffer 0.1 M (pH 7) containing 2% glutaraldehyde, 10 mM CaCl₂ and 10 mM MgCl₂. After 1 h incubation at 4°C and in the dark, samples were again centrifuged, rinsed and resuspended in 1 mL HEPES buffer 0.1M. Samples were stored at 4°C until analyses at the laboratory. Nile Red was added to each sample at a final concentration of 5 µg/mL sample, vortexed for 20 s and incubated 5 min at room temperature. The sample was then mounted onto a glass slide and observed on a Zeiss Observer Z1 epifluorescence inverted microscope using a DS Red filter cube (λ_{ex} : 550/25 nm; beamsplitter 570 nm LP, λ_{em} : 605/70 nm). The percentage of each diatom taxon in the Bottle net samples containing lipid droplets was then determined by scanning a counting a graduated Sedgewick Rafter chamber.

2.4.6. Spore induction and germination experiments

At station M2, larger amounts of resting spores and winter forms were observed for several taxa such as *Odontella weissflogii*, *Chaetoceros atlanticus*, *Eucampia antarctica* and *Proboscia inerme*, coinciding with a higher Si-limitation at this site with low Si/DIN (Dissolved Inorganic Nitrogen = nitrate + nitrite + ammonium) surface ratios (0.05-0.11). Hence, this site was chosen for exploratory experiments on resting spore induction and germination processes. At the first visit (M2-1), a spore induction experiment was carried out using 6 X 500 µL aliquots collected from the 100-450 m Bottle net sample. All aliquots were resuspended in 15 mL low nutrient water (collected at 30°S during transit to the study area) and three were placed in a dark incubator (low nutrient dark treatment) while the three others were placed in a lit incubator (50% of incoming surface light) cooled with running surface water. After 20 days, samples were fixed with acidified lugol and stored at 4°C. Resting spores and winter stages were enumerated back at the laboratory in all samples in an Utermöhl sedimentation chamber.

On the second visit at this site (M2-2), a spore germination experiment was conducted on the most frequently observed resting spores (*Odontella weissflogii*). Two times 15 resting cells of *O. weissflogii* were isolated under the microscope onboard from the 100-150 m Bottle net samples and resuspended in 10 mL filtered low nutrient water collected underway at 30°S. Both samples were placed in a lit surface incubator with no nutrient addition for the light treatment and +20 µM Si and +1 µM P for the light+nutrient treatment. After 12 days of incubation, samples were fixed with acidified lugol and stored at 4°C. Resting spores and vegetative cells were enumerated back at the ground-based laboratory in all samples in an Utermöhl sedimentation chamber.

2.5. Biogenic Silica (BSi)

An aliquot of 10 mL was filtered for biogenic silica (BSi) onto a 47 mm 0.6 µm polycarbonate filter, which was rinsed with milliQ water and dried at 60 °C for 24 h. Analyses were carried out in the laboratory following the triple NaOH/HF extraction procedure (Ragueneau et al., 2005) using spectrophotometry for Si measurements and fluorometry for Al measurements (Howard et al., 1986). This method allows to correct for possible BSi overestimation due to the dissolution of siliceous lithogenic

material during the first leaching. Particulate silica is expressed in mg Si using a converting factor of 28. Blank values, estimated from measurement of 8 independent samples were $0.54 \pm 0.4 \mu\text{g L}^{-1}$ for biogenic silica, $0.37 \pm 0.04 \mu\text{g L}^{-1}$ for lithogenic silica, and $0.04 \pm 0.03 \mu\text{g L}^{-1}$ for particulate aluminum.

2.6. Carbon content calculations

Carbon content was calculated for diatoms in all Phytonet and Bottle net samples based on intact and broken cells with visible cytoplasmic content, after size and shape measurements (minimum number of cells measured $n=25$) in light microscopy (following NF EN 166195, 2015). The carbon conversion formula from biovolume (in μm^3) was derived from Eppeley et al. (1970) modified by Smayda, (1978):

$$\text{Log}_{10} \text{ C biomass (pg C)} = 0.76 \times \text{Log}_{10} (\text{Biovolume}) - 0.352$$

For diatom resting spores of *Chaetoceros sp.* and *Odontella weissfloggii*, the biovolume to C biomass conversion formula of Kuwata et al. (1993) was used. For each sample, between 1,000 and 3,000 cells were counted in a graduated 1 mL Sedgwick-Rafter chamber.

3. Results

3.1. Characterization of deep particle stocks

Integrated and absolute particle abundances are presented in Fig. 3 and Table 2 respectively. Within the intermediate layer (i.e. 125-500 m), M1 exhibited the lowest particle (part.) abundances (3.1×10^7 part. m^{-2}) while the HNLC station M4 exhibited the highest abundances (2.6×10^8 part. m^{-2}). In this intermediate layer, abundances decreased at all sites between the first and last visits which occurred 11 to 15 days later, paralleling the demise of the bloom. The intermediate layer at the plateau station M2 could only be sampled between 100-450 m (1st visit), 125-450 m (2nd visit) and 125-375 m (3rd visit) which renders the comparison with the other stations more difficult. Nevertheless, according to the 125-450 m layer sampled during the second visit, we can fairly assume that particle abundances were intermediate (1.1×10^8 part. m^{-2}), being higher than M1 but lower than M3/M4. When expressed in number of particles per cubic meter (Table 2), we observe a clear decreasing trend with depth at all stations, except at M3-1 where particle concentrations were higher within the 125-500 m layer (6.1×10^5 part. m^{-3}) compared to the 60-125 m layer (4.0×10^5 part. m^{-3}). In the deep layers (i.e. > 500 m), particle concentrations ranged between 5.0×10^4 part. m^{-3} at M1 to 1.9×10^5 part. m^{-3} at M4-2.

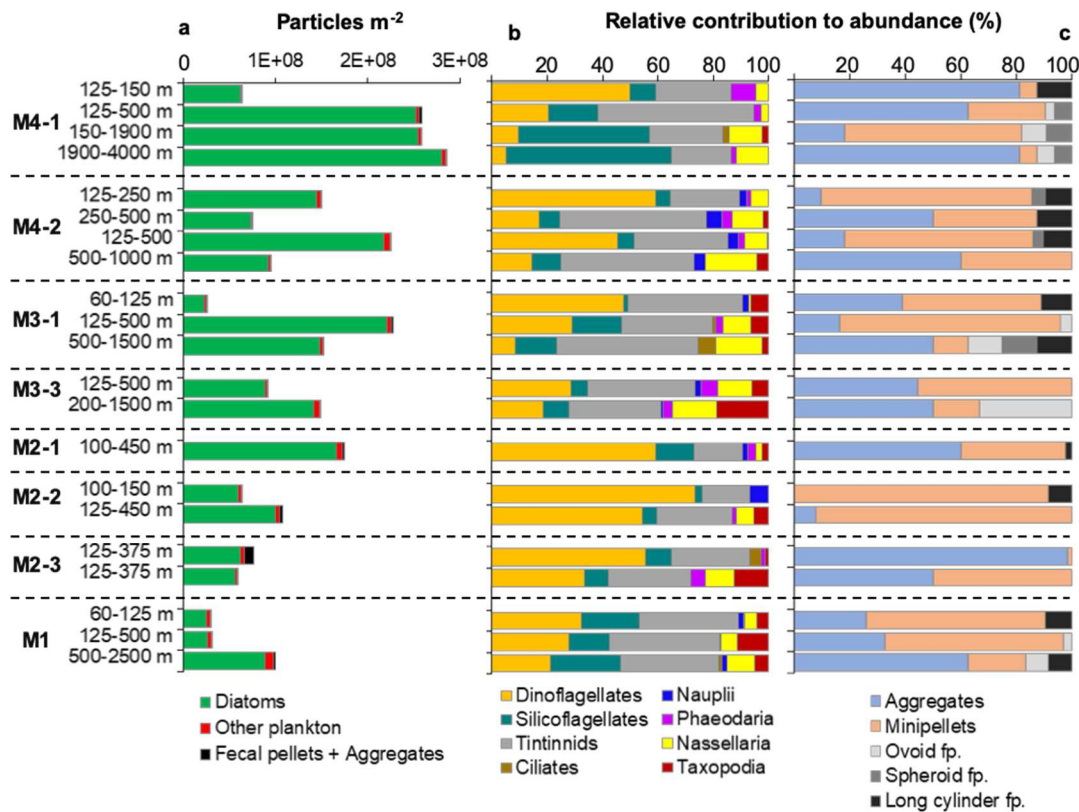


Figure 3: a. Integrated particles per m^{-2} for diatoms, other microplankton and fecal pellets+aggregates for all Bottle net casts at the four study sites. The integration depth is indicated on the left axis. b. Relative percent contribution of main lineages to the other microplankton groups (excluding diatoms) in all Bottle net casts. c. Relative percent contribution of different types of inert particles: aggregates, minipellets <50 μm , and three different types of fecal pellets (fp.).

Table 2 : Particle concentration (total cells + aggregates + fecal pellets) in particles m^{-3} for all Bottle net samples according to station and sampling interval.

Station	Integrated sampling depth (m)	Particle concentration (particle m ⁻³)
M1	60-125 m	468 032
	125-500 m	83 680
	500-2500 m	49 826
M2-1	100-450 m	499 935
M2-2	100-150 m	1 267 622
	125-450 m	331 988
M2-3	125-375 m	307 361
	125-375 m	236 546
M3-1	60-125 m	398 300
	125-500 m	606 904
	500-1500 m	151 480
M3-3	125-500 m	245 226
	200-1500 m	113 800
M4-1	125-150 m	2 523 000
	125-500 m	689 680
	150-1900 m	148 016
	1900-4000 m	135 767
M4-2	125-500 m	600 736
	500-1000 m	189 719

376

377 Regarding the type of particles collected, one of the most striking features was the
378 dominance of diatom cells at all sites and depths (Fig. 3a). On average, diatom cells
379 represented 93 ± 6 % ($n = 19$) of the total particle amount, while other microplankton
380 groups only represented 5 ± 4 %. Surprisingly, particles such as fecal pellets and
381 aggregates only contributed 2 ± 3 % of the total particle amount. The relative
382 abundance of microplankton other than diatoms was the highest at M1 reaching up to
383 16 % of the total particle amount within the 60-125 m layer. Aggregates, mostly large-
384 sized (100-400 μm) were the most numerous at M2-3 (125-375 m layer) contributing
385 14 % (1.0×10^7 part. m^{-2}) of the total particle amount while they did not exceed 1 %
386 at the other stations. Interestingly, those large aggregates were not observed within
387 the same layer sampled 8 h later, suggesting a short-lived export event.

388 Among identified microplankton groups, excluding diatoms (Fig. 3b), tintinnids ($35 \pm$
389 12 %) and dinoflagellates (34 ± 21 %) were dominant at most sites and depths.
390 Silicoflagellates were the following most abundant group (16 ± 15 %). They were
391 notably found to increase with depth and were the highest for the two deepest casts
392 at M4-1 (48 % at 150-1900 m, 60 % at 1900-4000 m) and at M1 (26% at 500-2500
393 m). Siliceous Rhizaria was the next most abundant group with a large diversity of
394 species belonging to different orders (e.g. mainly Nassellaria, Phaeodaria, and
395 Taxopodia). Nassellaria were present at all stations (8 ± 6 %) with the most abundant
396 species belonging to the Theoperidae, Plagoniidae and Artostrobiidae families. A
397 rarely mentioned Taxopodia, which has only one described species (*Sticholonche*
398 *zanclea*) was also very frequent at all sites and depths (5 ± 5 %). Phaeodarians were
399 also often present although in minor proportions (2 ± 2 %) and were mostly
400 represented by several *Protocystis* species (e.g. *Protocystis tridens*, *Protocystis*
401 *swirei*, *Protocystis balfouri*, *Protocystis harstoni*, *Protocystis micropilecus*). Although
402 minor contributors to the deep water particle stocks, they should play an important
403 role in the production of minipellets (Fig. 3c, Fig. 4a) and in particulate Si stocks as
404 their cellular quotas are higher than those of diatoms (Biard et al., 2018).

405 Among inert particles (Fig. 3c), identifiable fecal pellets (round, ovoid or elongated)
406 were negligible (10% on average for all casts) compared to aggregates and
407 minipellets, which both constituted 45% on average of the remaining particles (see
408 suppl. Fig. S4 for pictures of different types of particles). Minipellets are typically < 50
409 μm wide and are known to be excreted by *Protocystis* species (Gonzalez, 1992) that
410 was very abundant in surface Phytonets (data not shown). The occurrence of
411 Phaeodaria and their trophic behavior will be further discussed in another paper
412 (Leblanc et al., in prep). Here, minipellets were mostly constituted of diatom
413 fragments, mostly belonging to the species *Fragilariopsis kerguelensis* (Fig. 4a,
414 suppl. Fig. S4b), while *Protocystis* spp. were repeatedly observed in the Phytonet
415 samples with one or several whole ingested *F. kerguelensis* cells. Small aggregates
416 (<100 μm) were the most dominant type of aggregates and were also tightly packed
417 with crushed diatom debris, as well as coccoliths from *Emiliana huxleyi* in some
418 samples. Fecal pellets imaged by SEM revealed a very high content in biominerals,
419 mostly diatom frustule debris (Fig. 4).

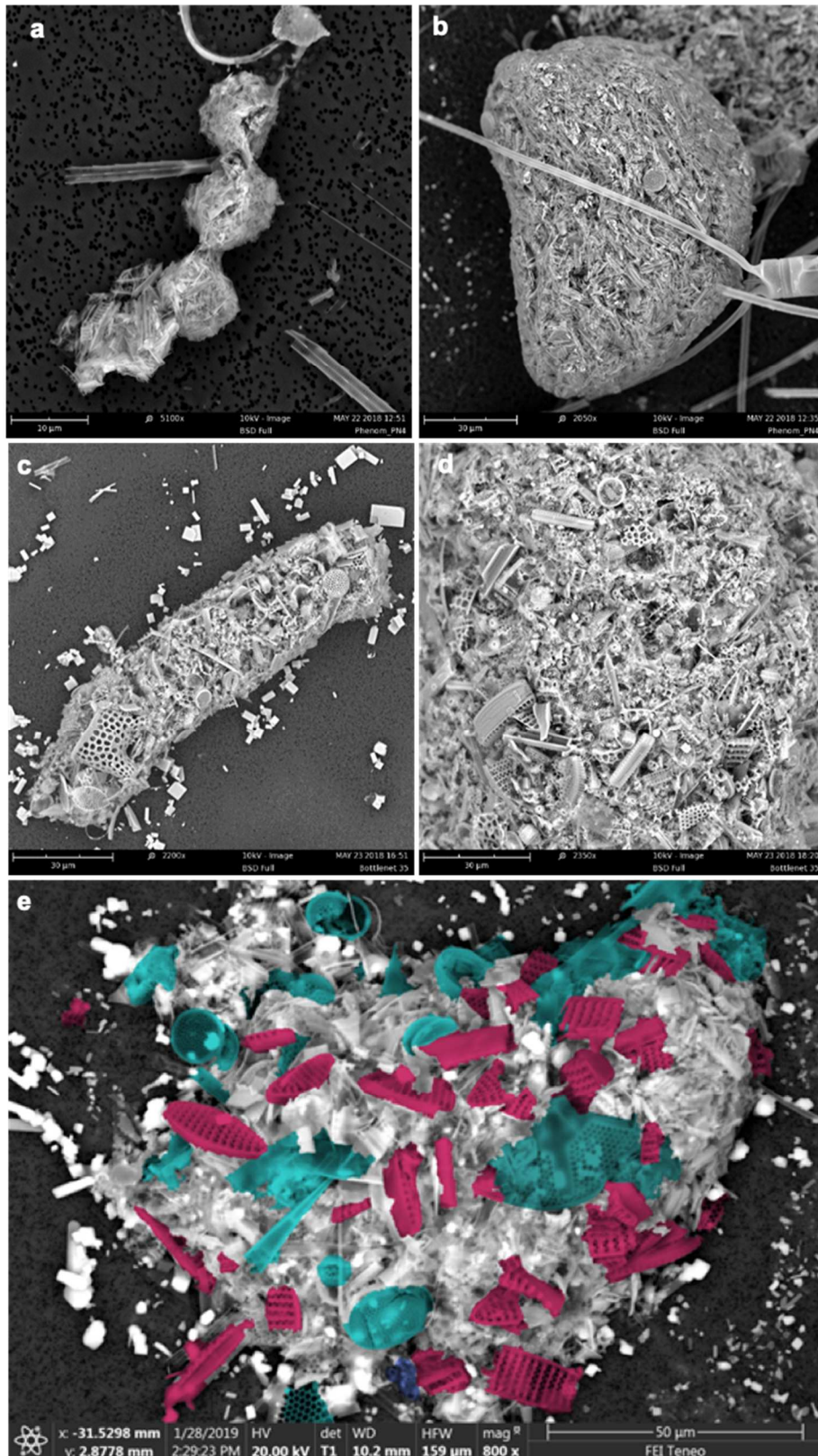
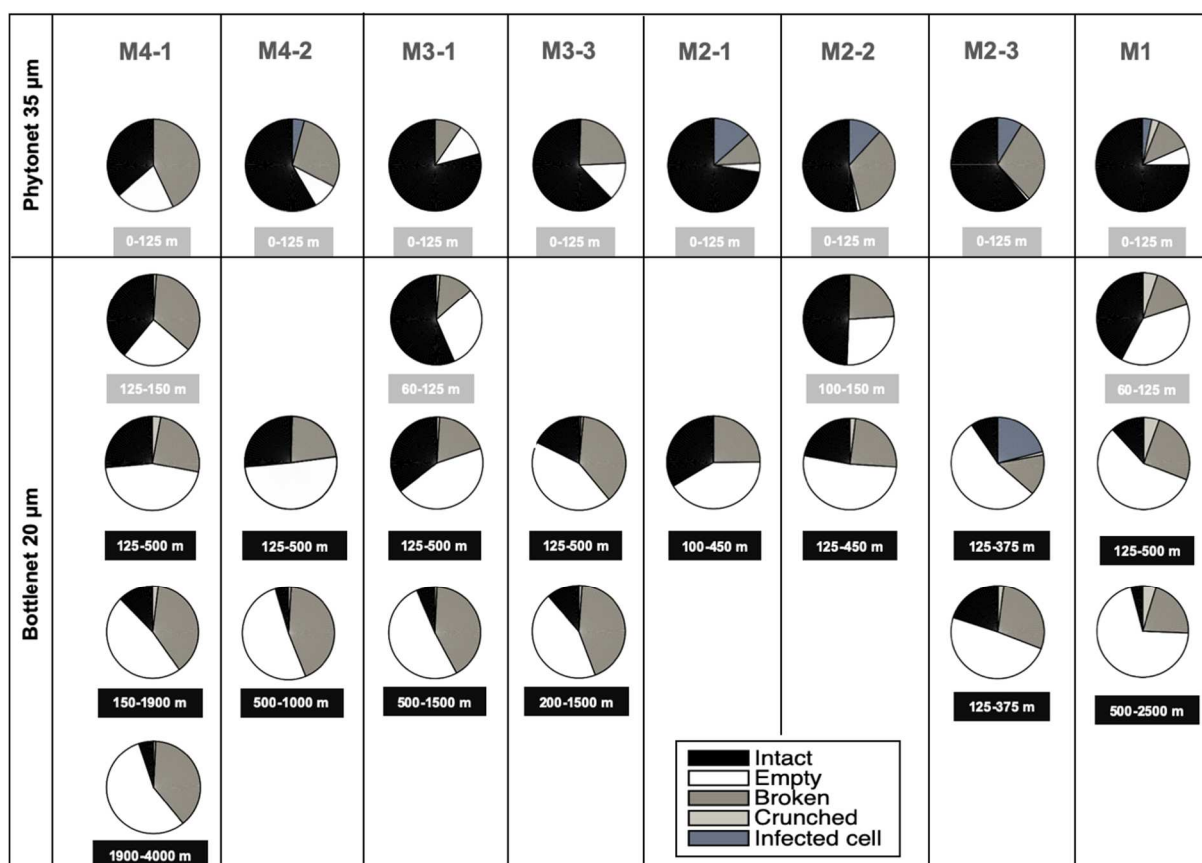


Figure 4: a. Phaeodarian minipellets, b. ovoid fecal pellet, c. long fecal pellet, d. zoom on a rounded fecal pellet content. e. Loose fecal pellet containing recognizable debris of *Fragilariopsis kerguelensis* (pink) and centric diatoms (turquoise). A few coccoliths are also visible (purple).

3.2. Diatom physiological state

The state of the diatom cells within the upper 0-125 m layer sampled by the Phytonet and the deeper layers sampled by the Bottle net is presented in Fig. 5. Within the upper 0-125 m layer, diatoms were mostly intact (62 ± 12 %) while the remaining frustules were broken (24 ± 11 %) or empty (9 ± 6 %). No large differences were observed between stations except at M4-1 where more broken frustules were observed (43 %). At the reference plateau station M2, a parasitic infection event was observed at the three visits, affecting almost exclusively the species *Corethron inerme* and to some lesser degree *Proboscia* and *Rhizosolenia*. The percentage of infected frustules varied between 14 % (1st visit) to 9 % (3rd visit) within the upper layer.

In Bottle net samples, the most conspicuous feature was the decreasing contribution of intact cells with depth, at all stations and visits. Within the intermediate layer (125-500 m), frustules were mostly empty (49 ± 5 %) or broken (26 ± 6 %) while intact cells were a minority (23 ± 8 %). In the deep layers located below 500 m, only few intact cells were still observed, contributing to 5 ± 1 % of the total cells. Crunched frustules indicative of mesozooplankton grazing were rare in most samples (< 3 %) although they were more frequent at M1 with a contribution of 5-6 % within the 60-



2500 m layer.

Figure 5 : Observed state of diatom cells in the Phytonet samples (upper panel) and in the Bottle net samples (lower panel) at each site and revisit. Collection depth is indicated below each pie chart (in grey for the surface layer between 0 and 125 m, in black below). See method section for “crunched” and “infected” definition.

449

450 At depth, infected cells were only observed at the last visit (i.e. M2-3, 21 % of the
 451 cells) within the 125-375 m layer. Interestingly, those infected cells were associated
 452 with large aggregates and were not found in the following cast performed 8 hours
 453 later.

454 *Viability test*

455 Results from the SYTOX Green labelling experiment showing the percentage of
 456 viable cells quantified on board immediately after sampling are presented in Table 3.
 457 The percentage of viable diatom cells decreased at all sites between revisits in both
 458 Phytonet and Bottle net samples. Within the upper 0-125 m layer, the percentage of
 459 viable diatoms was the highest at station M3 (64 % then 47%) indicating a good
 460 physiological state of the cells while it was the lowest at the eastern station M1 (18
 461 %) and above the plateau at M2 where a decreasing trend from 47 % (1st visit) to
 462 only 6 % (3rd visit) highlights the decaying stage of the diatom population even
 463 though visually intact cells represented a much larger contribution (Fig. 5). At the
 464 HNLC station M4 viable diatoms represented only a small third of total cells in the
 465 phytonet (28% then 26%). In the intermediate layer of M2 viable diatoms in the Bottle
 466 nets closely followed that of the Phytonets (43, 25 and 8 %). A larger proportion of
 467 live cells (64%) was found in a subsurface layer (125-150 m) at station M4-1 and this
 468 proportion was still fairly elevated in the deeper casts upon the first visit with 29 and
 469 24 % of viable cells in the 150-1900 and 1900-4000 m casts respectively. On the
 470 second visit however this proportion dropped substantially with only 4 % viable cells
 471 between 250-500 m and none in the 500-1000 m layer again suggesting the decay of
 472 the diatom population.

473

474 **Table 3:** Percentage of live diatom cells estimated after SYTOX labelling at each site and revisit and
 475 integrated sampling depths for the surface phytonet samples (0-125 m) and for Bottle net casts.

Station	Integrated sampling depth (m)	% live diatoms
M1	0-125	18
	125-500	11
	500-2500	1
M2-1	0-125	47
	100-450	43
M2-2	0-125	19
	125-450	25
M2-3	0-125	6
	125-375	8
M3-1	0-125	64
	125-500	20
M3-2	0-125	47
	125-500	12
M4-1	0-125	28
	125-150	64
	125-500	51
	150-1900	29
	1900-4000	24
M4-2	0-125	26
	250-500	4

3.3. Diatom community structure within surface and deep layers

Relative abundances

Diatom relative abundances from samples collected by both the Phytonet and the Bottle net are presented in Fig. 6. Results show a clear difference in diatom communities between the two stations located above the plateau (M2) and east of Kerguelen (M1) and the two stations located west of Kerguelen (M4 and M3). Within the upper 125 m layer, the Fe-fertilized plateau was dominated by *Corethron inerme* (81 ± 12 %) and *Proboscia* spp. (mostly *Proboscia alata*; 9 ± 3 %). At M2, the Phytonet contents closely matched the surface layer Niskin observations (Lafond et al., 2020) showing increasing abundances at each revisit of extremely long *Corethron inerme* filaments (up to 7-8 mm long, up to 74 cells in one filament) in the mixed layer (~80 m). At M1, some *Corethron* cells (13 %) were again observed in the surface Phytonet but this genus was not dominant while *Fragilariopsis kerguelensis* (42 %) and centric species constituted the bulk of diatom diversity.

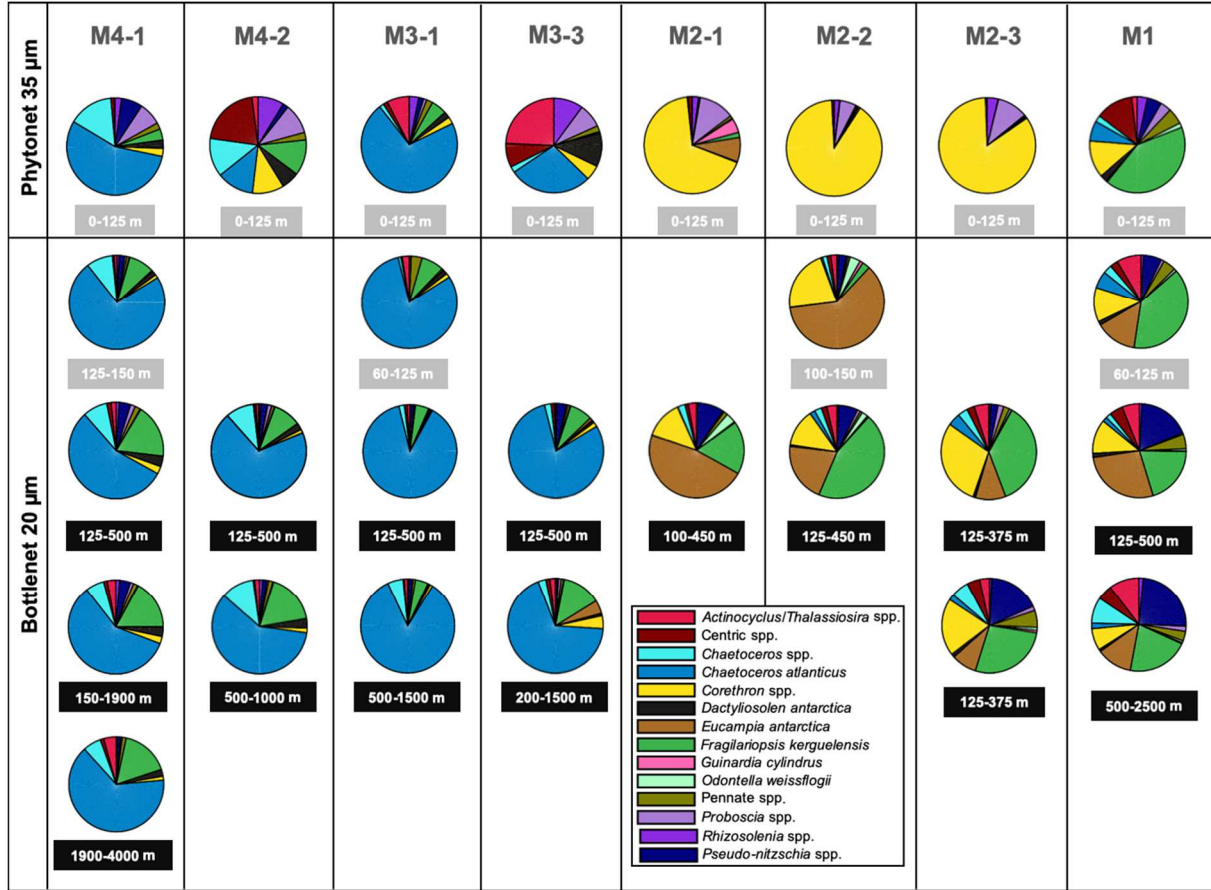
In the intermediate layer (125-500 m) at M2 and M1 the Bottle net samples reflected a very similar community that was dominated by a mix of *Eucampia antarctica* (30 ± 23 %), *F. kerguelensis* (26 ± 16 %), and *Corethron* spp. (19 ± 7 %) although the importance of *E. antarctica* declined throughout the survey period while the contribution of *C. inerme* increased with time at M2. Species belonging to the genus *Pseudo-nitzschia* (mostly *Pseudo-nitzschia heimii*) were also present contributing up to 18 % of the abundances at the last visit at M2 (125-375 m layer) and up to 25% in the deeper cast at M1 (500-2500 m). These results suggest that M1 was partly influenced by the nearby plateau despite its higher bathymetry, which is coherent with the water mass circulation pattern (Park et al., 2014).

By contrast, the surface layer of the western stations M3/M4 was dominated at the first visits by *Chaetoceros atlanticus* (64 ± 12 %), progressively replaced by a mix of different taxa at the second visit: *Chaetoceros atlanticus* (20 ± 11 %), other centrics (14 ± 9 % ; mainly unidentified centrics), *Actinocyclus/Thalassiosira* spp. (13 ± 16 %), *Dactyliosolen antarctica* (9 ± 4 %), *Proboscia* spp. (9 ± 1 %), *Rhizosolenia* spp. (9 ± 1 %), and *Corethron* spp. (8 ± 4 %). Diatom communities were much less diverse within the intermediate and deep layers and largely dominated by *Chaetoceros atlanticus* (71 ± 11 %), followed by *F. kerguelensis* (11 ± 5 %). Other *Chaetoceros* spp., mostly *Chaetoceros dictyota* were also non negligible contributors to abundances at M4 (8 ± 2 % at both visits).

Winter stages and resting spores

The heavily silicified *Chaetoceros atlanticus* was a key species at the western stations M3/M4. It occurred under several forms: long chains composed of vegetative cells, a solitary stage with sigmoidal setae, which is likely a resting cell form, and under the 'bulbosum' form, which is thought to be the resting spore stage for this species (suppl. Fig. S3). In the surface layer the vegetative stage was dominant at

M4/M3/M1 but the solitary sigmoidal stage was also present even though less abundant. Interestingly, the '*bulbosum*' stage was never observed in the Phytonet samples but was abundant in the subsurface Bottle net samples at M4-1 (125-150 m), M4-2 (125-250 m), M3 (65-125 m) and M1 (65-125 m), suggesting a sporulation event occurring below the mixed layer although we cannot exclude that the



'*bulbosum*' form was not retained by the 35 µm mesh size of the Phytonet. The '*bulbosum*' stage was also present albeit at lower abundances in almost all the deepest Bottle net casts.

Figure 6: Relative contribution of diatom main taxa to abundance (comprising both intact and empty cells) in the Phytonet samples (upper pannel) and in the Bottle net samples (lower pannel) at each site and revisit. Collection depth is indicated below each pie chart (in grey for the surface layer between 0 and 125 m, in black further below).

Winter stages of another heavily silicified species *Eucampia antarctica* (suppl. Fig. S3), as small rectangular forms (Fryxell and Prasad, 1990), were quasi absent from the Phytonet samples, which could also be due to the mesh size exceeding their average size (15-30 µm), but were on the other hand very abundant in the subsurface casts starting below 100 m at M2 and M1 in the Bottle net samples. This small winter form was minor at M3 and quasi absent at M4.

Several *Odontella weissflogii* morphotypes were also observed during the cruise. The vegetative lightly silicified stage was quasi absent from all samples while a rectangular form much more silicified than the vegetative stage and with short apical horns was the dominant form. This stage has been identified as the resting spore stage of *O. weissflogii* (Scott and Marchant, 2005) but a complete description of this stage is lacking so far. We also observed a larger rounder stage with even shorter apical horns, and therefore hypothesize that the rectangular form may be a resting cell or transition stage towards the actual resting spore, which would be the rounded form (suppl. Fig. S3). Both forms were absent at station M4 and M3 while the resting stage was most abundant at M2 and M1 in the upper Bottle net casts. The round spore stage was on average 10 times less abundant than the rectangular stage and was found at the same sites.

The small *Proboscya inermis* winter stages and abnormal forms (10-25 μ m) of this stage (suppl. Fig. 2 in Lafond et al., 2020) were the next contributors to winter/resting stages but were much less abundant, even though present at all sites, with a dominance at M4.

Several forms of *Rhizosolenia* with heavily silicified otaria- and clasper-lacking forms such as *Rhizosolenia polydactyla f. squamosa* are thought to be resting spore/stage employed for overwintering but there is still a debate as to whether these morphotypes are winter resting stages or actual resting spores (Armand and Zielinski, 2001 and refs therein). This stage was present but as a very minor contributor in Phytonecks and in one shallow Bottle net.

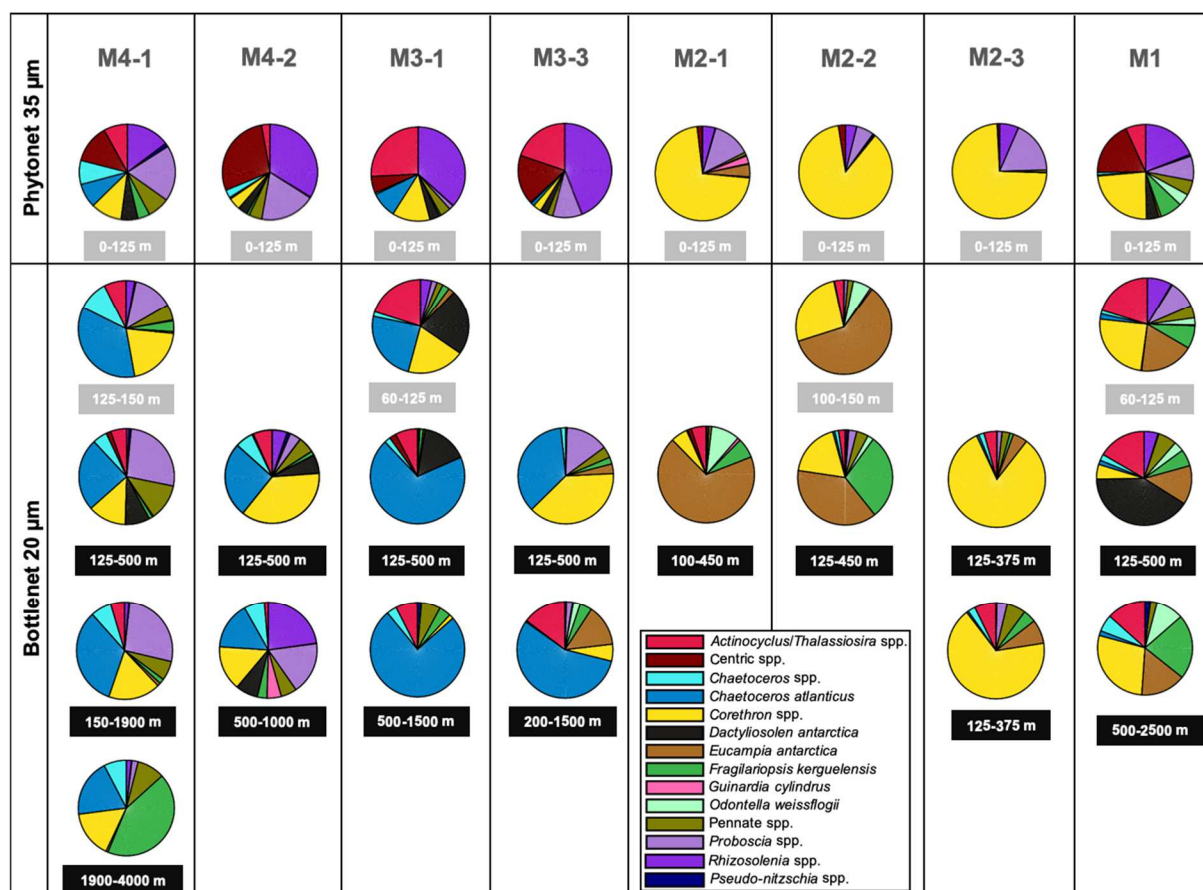


Figure 7: Relative contribution of diatom main taxa to C biomass (comprising intact cells only) in the Phytonet samples (upper pannel) and in the Bottle net samples (lower pannel) at each site and revisit. Collection depth is indicated below each pie chart (in grey for the surface layer between 0 and 125 m, in black further below).

3.4.Si and C concentrations and integrated stocks in the intermediate and deep layers

BSi and diatom C biomass in Bottle nets

Average and integrated biogenic silica and diatom carbon concentrations over the Bottle net sampling layers are presented in Table 4. Average concentrations of diatom C measured from intact cell counts were expectedly the highest in all subsurface casts, with a maximum value of $556 \mu\text{g C m}^{-3}$ over 100-150 m at M2-2 (main contributor *E. antarctica*) followed by M4-1 over 125-150 m with $389 \mu\text{g C m}^{-3}$ (main contributor *C. atlanticus*). M1 and M3 subsurface casts over 60-125 m contained much less intact diatoms with 128 and $74 \mu\text{g C m}^{-3}$ respectively. Diatom C content then decreased at all sites with depth and reached the lowest values ($1-6 \mu\text{g m}^{-3}$) in all casts extending to over 1000 m depth. The highest concentrations for the intermediate layer (between 125 and 500 m) were found at M2-1 and M4-1 but decreased upon revisits to the same stations. Integrated diatom C values ranged between 1 and 40 mg C m^{-2} over the considered sampling layer with the highest integrated diatom C content measured at M2-1 (40 mg C m^{-2}) over 100-450 m followed by M4-1 (33 mg C m^{-2}) over 125-500 m. The lowest value for the intermediate layer was measured at M1 (2 mg C m^{-2} over 125-500 m).

Outside the plateau, BSi concentrations in the intermediate layer were highest at M4 (46 mg Si m⁻³) followed by M3 (18-12 mg Si m⁻³) and M1 (15 mg Si m⁻³). At M2 it reached 49 mg Si m⁻³ at the third visit within the 125-375 m layer. Integrated concentrations were the highest at M4-1 in the intermediate (17,272 mg Si m⁻²) meso- (42,277 mg Si m⁻²) and bathypelagic (28,374 mg Si m⁻²) layers suggesting a more efficient export of Si in HNLC waters. At M2, integrated concentrations increased steadily between the first (2,088 mg Si m⁻²) and last visit (12,168 mg Si m⁻²) although the integrated depth was lower, which means that the Si stock had increased significantly at depth.

Table 4: Amounts of intact diatom C (from microscopical counts) and total biogenic silica (from chemical measurements) in Bottle net samples (>20 µm) calculated as an average concentration (per m⁻³) in the considered layer or as integrated values over the sampling depth (per m⁻²).

		[diatom C]	Σdiatom C	[BSi]	ΣBSi
		µg C m ⁻³	mg m ⁻²	mg Si m ⁻³	mg Si m ⁻²
M4-1	125-150 m	389	10		
M4-1	125-500 m	89	33	46.1	17 272
M4-1	150-1900 m	7	13	24.2	42 277
M4-1	1900-4000 m	2	4	13.5	28 374
M4-2	125-250 m	148	19		
M4-2	250-500 m	13	3	24.1	6031
M4-2	500-1000 m	6	3		
M3-1	60-125 m	74	5		
M3-1	125-500 m	38	14	18.0	6753
M3-1	500-1500 m	2	2	4.8	4780
M3-3	125-500 m	14	5	12.0	4848
M3-3	200-1500 m	3	4		
M2-1	100-450 m	115	40	6.0	2088
M2-2	100-150 m	556	28		
M2-2	125-450 m	30	10	25.2	8179
M2-3	125-375 m	76	19		
M2-3	125-375 m	35	9	48.7	12168
M1	60-125 m	128	8		
M1	125-500 m	5	2	15.0	5639
M1	500-2500 m	1	1	5.6	11236

Relative carbon biomass

Taxon-specific contribution to carbon biomass of intact cells only is presented in Fig. 7. Above the Kerguelen Plateau at M2, carbon biomass follows the same trend as abundances, with *Corethron inerme* (77 ± 8 %) and *Proboscia* spp. (12 ± 6 %) being the main contributors within the upper 125 m layer. Below 125 m, *Eucampia antarctica* contributed to 69 % of C biomass at the first visit before its biomass decreased significantly at the third visit, when it was replaced by *C. inerme* (67-83 %). *Odontella weissflogii* as resting cells and/or spores contributed to 10 % at the first visit and decreased with time while *Fragilariopsis kerguelensis* contributed to 29 % at the second visit.

At the eastern station M1 *Corethron* spp. (24 %) was also an important contributor in the upper 125 m layers but other taxa also drove the C biomass: *Rhizosolenia* spp.

(19 %, e.g. *Rhizosolenia simplex*, *Rhizosolenia curvata*), and other centrics (18 %, e.g. *Asteromphalus hookeri*, *Actinocyclus octonarius*, *Azpeitia tabularis*, *Coscinodiscus* spp., unidentified centrics). Below the surface layer key species contributing to C biomass were similar to M2 (i.e. *C. inerme*, *E. antarctica*, *F. kerguelensis*), although species belonging to *Actinocyclus/Thalassiosira* complex became important (17 ± 3 % within the three sampled layers) and the species *Dactyliosolen antarctica* dominated C biomass in the intermediate 125-500 m layer (41 %).

At the western stations M3/M4, the biomass of large centric species became dominant although they were numerically few. Indeed, within the upper 125 m layer, *Proboscia* spp. (mainly *Proboscia alata*), *Rhizosolenia* spp. (e.g. *R. curvata*, *Rhizosolenia polydactyla* f. *polydactyla*), *Actinocyclus/Thalassiosira* spp. (e.g. *Actinocyclus curvatulus*, *Actinocyclus octonarius*, *Thalassiosira lentiginosa*, *Thalassiosira tumida*), and other centrics (e.g. *Asteromphalus hookeri*, and unidentified centrics) contributed together to 78 ± 8 % of C biomass. In the intermediate layer, *Chaetoceros atlanticus* (39 ± 21 %) was the main contributor to C biomass followed by the large centrics *Corethron* spp. (22 ± 19 %, mainly *Corethron pennatum*), *Proboscia* spp. (11 ± 12 %, mainly *P. alata*), and *Dactyliosolen antarctica* (8 ± 6 %). A similar pattern extended to the deep layers with *Chaetoceros atlanticus* still driving C biomass except within the deepest layer sampled during the cruise (M4-1, 1900-4000 m) where *Fragilariopsis kerguelensis* contributed up to 43 % of the C biomass.

3.5. Diatom lipid content

The proportion of each diatom species containing lipid droplets (as stained with Nile Red) is presented in Fig. 8. *Fragilariopsis kerguelensis* appears to be the taxon that is most likely to sink out of the surface layer with lipids and its contribution to total stained cell was major (70-80%) at M4-1 and M1. *Chaetoceros atlanticus* mostly in the form of single cells undergoing a sigmoidal stage or as spores (*C. atlanticus bulbosum*) was the next major taxon containing lipids particularly at M3. At M2 *Eucampia antarctica* as well as *Corethron inerme* were also often showing lipid droplets, their relative contribution being similar to the evolution of total frustule abundance over the three visits. Finally *Odontella weissflogii* resting stages/spores were also important lipid contributors during the first two visits at M2.

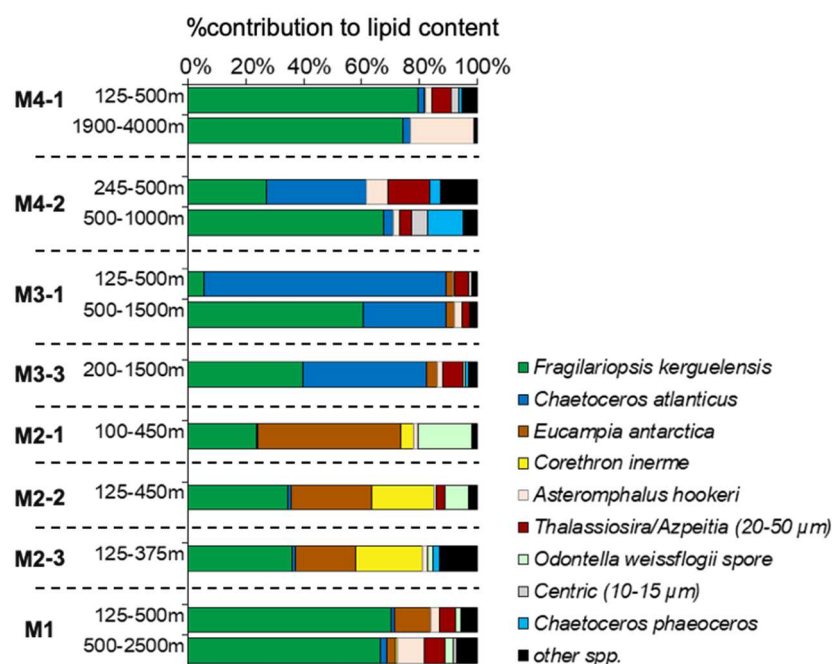


Figure 8: Relative contribution of main diatom taxa to lipid content, based on enumeration of cells positively labelled with Nile Red. Taxa contributing to less than 3 % of lipid containing cells were pooled together in the category “other spp.”

3.6. Spore germination and induction experiments at M2

Spore germination. At M2-2, 2 X 15 resting cells were collected from a subsurface Bottle net opened between 100 and 150 m. After 12 days incubation, the aliquot incubated with both light and nutrients (+Si+P) showed a successful germination of all resting stages, and the number of cells amounted to 6,072 of actively dividing *Odontella weissflogii* vegetative cells (Table 5). Cells looked healthy and no empty frustules were found. In the light-only treatment the 15 initial cells yielded 3 times less vegetative cells with a total of 2,048 cells. Some resting cells remained in the sample (10) and could be either the ungerminated initially isolated resting cells or new resting cells formed over the course of the incubation.

In addition, 758 larger, rounder forms of *Odontella* resting cells, suggesting a transition towards a resting spore stage, were counted in this treatment only, accounting for another 1/3 of cells. Several abnormal valves and half vegetative/half resting spore cells were also observed (see suppl. Fig. S5). Assuming that all resting cells germinated in the first treatment, the total amount of >6,000 cells in 12 days is achieved with a growth rate of 0.5 d⁻¹. In the light-only treatment, assuming that only 5 out of the 15 resting cells germinated (since 10 intact resting cells were still observed in the sample), the final amount of >2,000 cells is also achieved with a growth rate of 0.5 d⁻¹.

Table 5: Results of the spore germination experiment at M2-2 after 12 days incubation of 2 replicate samples containing 15 resting cells/spores of *Odontella weissflogii* in a light + Si + P and in a light-only treatment.

<i>Spore germination experiment</i>	Light +Si +P		Light only	
	Live	Empty	Live	Empty
<i>Odontella weissflogii</i> vegetative	6072	0	2048	78
<i>Odontella weissflogii</i> resting cell	0	2	10	6
<i>Odontella weissflogii</i> round form	0	0	758	0
<i>Total Odontella weissflogii</i> cells	6072	2	2816	84

Spore induction. At M2-1, 6 X 500 µL aliquots from the 100-450 m Bottle net were incubated in low nutrient water (LNW) + light or in low nutrient water and dark conditions for 20 days. Results are summarized in Table 6. In the LNW+dark treatment, about 30% more *Odontella weissflogii* resting cells and rounded forms were observed at the end of the incubation showing a higher probability to form spores in environments deprived of both nutrients and light. A similar trend was observed for *Eucampia antarctica* winter forms, which were 3 times more abundant in this treatment as well.

Table 6: Results of the spore induction experiment at M2-1 after 20 days of incubation of 2X3 replicate samples collected from phytonets and incubated in low nutrient water (LNW) in surface light conditions and in the dark.

<i>Spore induction experiment</i>	LNW + light treatment		LNW + dark treatment	
	Live	Empty	Live	Empty
<i>Odontella weissflogii</i> resting cells	64	81	91	65
<i>Odontella weissflogii</i> resting spores (round form)	4	9	9	5
<i>Eucampia antarctica</i> winter form	99	305	297	500

4. Discussion

4.1. Nature and mode of export of the deep particle stock

The number of identifiable individual diatom frustules collected with the Bottle net in deep waters around Kerguelen islands by the end of summer was not negligible (10^7 - 10^8 cells m^{-2}) and the deep diatom stock (below 125 m) was one order of magnitude higher than the stock present in the upper (0-125 m) layer (Lafond et al., 2020). It was also 3 orders of magnitude higher than the concentration of single phytoplankton cells measured on average by Agustí et al. (2015) in the 2,000-4,000 m layer in the subtropical Ocean. This is not surprising considering the large annual diatom bloom event occurring around Kerguelen Islands due to natural Fe-fertilization, which has been documented during previous cruises in the same area (Armand et al., 2008a; Lasbleiz et al., 2016), and given the shallower sampling depths. The export of diatom cells at depth was also expected considering that the MOBYDICK cruise occurred at the end of summer during the demise of the bloom, as previously documented from sediment trap samples in the same region (Rembauville et al., 2015), from sediment trap material over the Crozet plateau region (Salter et al., 2012; Salter et al., 2007), or further into the Australian sector of the Antarctic Zone (Rigual-Hernández et al., 2016; Rigual-Hernández et al., 2015). On the other hand, the dominance of single diatom cells (93%) over any other type of particles such as fecal pellets,

phytodetritus, and aggregates was unexpected. We have no other elements of comparison regarding the contribution of aggregates and fecal pellets in the subtropical ocean as these were not reported in Agusti's Bottle net study.

Given the size of the dominant taxa observed in our study (20-50 μm), it is unlikely that single cells sank to depth without being integrated to larger aggregates (Laurenceau-Cornec et al., 2020). It is possible that the Bottle net sampling could have promoted the disaggregation of phytodetritus during the upcast and water flow through the 20 μm net, potentially explaining the very low contribution of aggregates and fecal pellets. However, the condition of cells observed by microscopy directly after sampling on board, the absence of large mucus/TEP aggregates and the morphological shape of diatoms and other cells (frustules and setae intact) suggest that these particles were likely not aggregated at the time of sampling. The similarity of the taxonomic diatom composition in the Bottle nets compared to the above surface layer phytonets (Fig. 6) furthermore suggests a rapid export mode of diatoms over the plateau, which has already been hypothesized from similar diatom community structures between the surface layer and sediment traps moored at 300 m (Blain et al., 2020). We therefore hypothesize that the cells we observed sank rapidly out of the surface layer in loose phytodetritus aggregates, which disaggregated *in situ* at depth prior to collection. If shear stress or bacterial mineralization of TEP/colloids holding aggregates were initial hypotheses for particulate fragmentation in the water column, a study conducted by Alldredge et al (1990) concluded that biological processes such as animal grazing, were far more likely to mediate disaggregation processes (Alldredge et al., 1990 and references therein). However, due to the periodic vertical mixing linked to the passage of internal waves generated by the tide (also responsible for iron fertilization on the shelf) (Blain et al., 2007), a direct effect of turbulence cannot be excluded as the aggregates are brought closer and closer to the bottom.

Clearly, these cells were not exported as fecal pellets, given for instance the state of *Chaetoceros atlanticus* sigmoidal stages with unbroken setae, particularly in the deep cast (1900-4000 m) at M4-2. Microscopic examinations also allowed to observe loose aggregates still holding together as well as intact tightly packed fecal pellets (suppl. Fig. S4) which suggests that the Bottle net sampling did not substantially disrupt particles or aggregates.

On one occasion, at one of the two 125-375 m casts performed at M2-3, numerous large aggregates were observed (14 % of total particles but representing practically the entire inert particle fraction) together with cells covered with loose organic material. Unfortunately, it was complicated to estimate their C biomass due to their heterogeneity (density, composition, fractal structure) but their contribution to C biomass was likely not negligible for this cast since most of the other particles were empty diatom frustules. Interestingly, those large aggregates were not observed in the exact same layer 8 hours later (decrease in abundance by a factor X100) indicating a very brief export event at a high sinking rate. This station was sampled few days after a strong storm event which could have promoted both their physical aggregation through vertical mixing and their rapid export. Their disappearance 8 hours later further suggests an export event in the form of loose aggregates that

were not cohesive enough to persist below the surface layer. This observation could reconcile our data showing mainly single cells in the intermediate layers, with the mechanism proposed by Blain et al. (2020) in our study area of rapid export by aggregates formed at the surface. Once a critical threshold of cell concentration and stickiness is reached, this process would lead to a rapid flushing of the surface layer of diatoms in the form of aggregates, which then dissociate further down the water column. In another study carried out in the Australian sector of the Antarctic Zone, sediment trap data results also suggested a fast and relatively undisturbed downward transport of particles between 2000 and 3700 m and sinking velocities of $210 \text{ m}^2 \text{ d}^{-1}$ of the major diatom taxa were estimated (Rigual-Hernández et al., 2015).

Phytodetrital aggregates were previously reported to contribute significantly to export fluxes in this region. During ANTARES I, a thick fluff layer containing high pigment levels (up to $13 \mu\text{g L}^{-1}$) was observed west of Kerguelen at more than 3,000 m depth (Riaux-Gobin et al., 1997) while during spring (KEOPS 2), phytodetrital aggregates were the most abundant type of particles collected by polyacrylamide gel sediment traps over the Kerguelen plateau (Laurenceau-Cornec et al., 2015). A study of surface sediment samples in the same area during the spring bloom in 2005 (KEOPS 1) also revealed a number of intact diatom frustules on the seafloor suggesting an efficient transport mode of single cells at depth (Armand et al., 2008b) not excluding however our hypothesized sequence aggregation–sinking–disaggregation.

Finally, due to the very short period of particle collection (during a CTD upcast), we cannot exclude that we missed other important pulse export events such as the one observed at M2-3 especially at the end of the productive season, which is often characterized by an intense and brief export event called the "fall dump" (Kemp et al., 2000; Quéguiner, 2013).

4.2.Mortality modes

Parasitic infection

During the cruise, the diatom contribution to C biomass was the highest above the plateau at M2 (Table 4). An important development of long filaments of *Corethron inerme* occurred in the course of three successive visits over nearly a month and resulted in a doubling of diatom C biomass over the 0-100 m layer. This species was also mixed with a few (<10%) other large size tubular centrals such as *Rhizosolenia* spp. and *Proboscia* spp., which likely occupied the same ecological niche. During live observations on board at station M2 parasitic infection of many cells was clearly visible with some cells filled with small black parasites < 1 μm in size (suppl. Fig. S2). This was the only site (except a single occurrence at M4-2) where such parasitic infection was observed. Single cell sequencing of isolates picked on board and co-occurrence network analyses suggest that these parasites belong to the Syndiniales group, which was not previously known to infect diatoms (Sassenhagen et al., 2020). Interestingly, at M2-1, *Corethron* was only a minor contributor to the intermediate layer stocks, which was initially dominated by *Eucampia*. The relative contribution of *Corethron* at intermediate depth increased over time probably reflecting the sinking of infected cells as is visible on the third visit (15% of infected *Corethron* cells observed in the 125-375 m layer). The percentage of viable cells in the surface samples

decreased from 47 % on the first visit to 6 % on the last one (Table 2) reflecting massive cell mortality, which is likely the result of this parasitic infection. The apparition of infected cells below the euphotic layer at M2-3 could be the result of subsequent sinking of cells losing their membrane integrity and their buoyancy but could also be linked to the strong storm event occurring between M2-2 and M2-3 that disrupted the surface layer and induced mixing with the intermediate layer. It is however not clear from our results if the parasitic infection led to preferential sinking of *Corethron* empty cells or if this was just the result of the temporal increase of *Corethron* abundance over the three visits and mixed layer disruption following the storm.

Virus-mediated mortality of phytoplankton (killing-the-winner scenario) cannot be ruled out although we do not have precise data on this mechanism. Although estimates of the role of the viral shunt in the biological carbon pump are still uncertain, Suttle (2007) suggests a mortality of approximately 20% of the biomass of marine microorganisms per day on a global scale. A recent study conducted in the North Atlantic also indicated that viral infection of a ballasted biomineral containing phytoplankton such as *Emiliania huxleyi* appeared to stimulate vertical export flux and rather enhanced the biological C pump (Laber et al., 2018). Recent findings also indicate that viral infection of the bloom-forming genus *Chaetoceros* could induce mass formation of resting spores as a defense strategy (Pelusi et al., 2020), which is a mechanism that could lead to mass carbon export events by diatom spores. Other types of infections were observed during live observations of net material on board such as small nanoflagellate swimmers invading *Rhizosolenia spp.* cells or parasites flowing out of a *Ceratium lineatum* cell, which suggests that parasitic infections were actively occurring over the plateau at the end of the productive season. Zoosporic and fungal parasitic infection, in addition to viral and bacterial infection, are still a large unknown in our comprehension of diatoms as well as other processes leading to phytoplankton's bloom termination and are thought to be much more abundant than reported in the literature (Gutiérrez et al., 2016; Scholz et al., 2016). Si limitation has furthermore been shown to facilitate viral infection of diatoms in a highly productive coastal system (Kranzler et al., 2019). In our study, parasitic infection was also observed at the most Si limited station (Si:N ratios of 0.05-0.11) and we hypothesize that the thinner frustule observed at the station most depleted in silicic acid could also have facilitated the parasitic infection of large cylindric centrics such as *Corethron*, *Rhizosolenia* and *Proboscia*.

Grazing processes by microzooplankton

The high contribution of both dinoflagellates and tintinnids in the microplankton compartment and the dominance of small-sized (<100 µm) aggregates over fecal pellets in the Bottle net samples is consistent with the dominance of an active microbial food web reflecting the demise of the bloom rather than a mesozooplankton-dominated food web. This is similarly to what was observed by Landry et al. (2002) in the Polar Front region after the collapse of a large diatom bloom. Interestingly, minipellets (<30 µm) produced by Rhizaria were a major part of

the detrital stock in all Bottle net samples, with an average of 45% of inert particles (Fig. 3). Their origin was confirmed by direct observations on board (suppl. Fig. S4) of active grazing on diatoms by the phaeodarian group dominated by *Protocystis* spp. (mostly *P. swirei* and *P. tridens*). This group is known to feed on bacteria, algae and also fecal pellets or organic matter aggregates (Gowing, 1989; Gonzalez, 1992). We observed numerous small-sized (80-160 μm) *Protocystis* ingesting whole cells of *Fragilariopsis kerguelensis* and excreting minipellets comprised between 10-30 μm , filled with *F. kerguelensis* debris as well as with other undetermined cells. Such an active grazing by phaeodarians on diatoms associated to the production of minipellets has seldom been reported except in older studies in the Pacific Ocean (Gowing and Silver, 1985), and in the Southern Ocean off the Antarctic peninsula (Gonzalez, 1992) and in the Weddell Sea (Gowing, 1989). Despite their small numerical abundance, this group, together with other siliceous Rhizaria, could have an important contribution to the Si stocks measured in the Bottle net, given their elevated skeleton Si content (in our study 2.4 nmol Si cell⁻¹) compared to diatoms (e.g. see Brzezinski, 1985), and their ability to concentrate Si debris in minipellets (Nakamura and Suzuki, 2015 and references therein; Leblanc et al., in prep.). The ecological role of these phaeodarians is likely to be significant as evidenced by previous studies (Gonzalez, 1992), but it has received little attention until very recently, when new studies based on DNA metabarcoding have revealed the global importance of Rhizaria (Stukel et al., 2018) and phaeodarians in the particle vertical export (Gutierrez-Rodriguez et al., 2019). In a survey from 1988 in the Scotia Sea and the Weddell-Scotia confluence, integrated minipellets reached 10⁶ m⁻² values and were 5 orders of magnitude more abundant than krill feces (Gonzalez, 1992). In the Weddell Sea, phaeodarians were in turn actively grazed by salps such as *Salpa thompsoni* (Gowing, 1989), thereby linking the microbial food web to higher trophic levels. Other phaeodarians such as *Phaeodina antarctica* were also observed in our study and agglutinated both whole diatom valves and silicoflagellates skeletons, resulting in elevated particulate Si cell⁻¹. Hence Rhizaria, through their siliceous skeletons and fecal pellets, and specifically minipellets, appear as active contributors to the downward Si flux at the end of the productive season.

Grazing processes by mesozooplankton

Mesozooplankton abundance was on average higher during the spring cruise (58 to 1,249 x10³ ind. m⁻²) that took place in 2010 in the same area (KEOPS 2), compared to this study (64 to 860 x10³ ind. m⁻², A. Delegrange pers. comm.) reflecting the lower food availability in the surface layer at the end of summer. Despite the relatively small contribution of fecal pellets to the detrital deep stocks in the Bottle net samples signs of active mesozooplankton grazing (probably by copepods, which was the dominant zooplankton group or amphipods like *Themisto gaudichaudii* frequently observed from micronekton sampling) were clearly indicated by the presence of crunched frustules debris outside as well as inside fecal pellets. Potential prey selection was observed as crunched frustules were only observed for *Fragilariopsis kerguelensis* and several centric diatoms such as *Thalassiosira lentiginosa*, *Azpeitia tabularis* and *Asteromphalus hookeri* (suppl. Fig. S1). Other dominant diatoms such as *Eucampia*

antarctica, *Corethron inerme* or *Chaeroceros atlanticus* were never observed with crunch marks even though they were observed in fecal pellets suggesting different types of grazer feeding behavior. During the EIFEX Fe-fertilization experiment, Assmy et al. (2013) reported that the thick frustules of *F. kerguelensis* made them less palatable for mesozooplankton and crunched end cells were interpreted as a result of copepods being deterred by the high energy expenditure needed to crush these preys (Hamm et al., 2003). Yet, in our study, fecal pellets observed in SEM also contained a number of crushed (and sometimes whole) *F. kerguelensis* valves together with other similarly heavily silicified diatoms such as *E. antarctica*, *C. atlanticus*, *Corethron criophilum* as well as many small intact *Chaetoceros* resting spores indicating active ingestion by grazers (Fig. 4). It is possible that the high lipid content of these species (Fig. 8) made them more palatable for zooplankton upon entering the winter diapause period. As a general rule, SEM observations of <100 μm fecal pellets and the diverse community observed within (through numerous identifiable frustules, see Fig. 4) suggest that even diatoms with thick frustules are actively grazed by copepods and other mesozooplankton species. However, we were not able to identify whether the preferential downward pathway for *F. kerguelensis* was sinking as single cells or included in fecal pellets. Furthermore, pulverized frustule debris were commonly observed during on board examinations but could not be quantified. Improved techniques would be needed to isolate fecal pellets, quantify their relative Si vs. C contents together with a precise taxonomic identification of frustule remains. Clearly, the Si/C ratio of these fecal pellets should be disproportionnally high compared to the single cell flux, even though the latter was dominated by empty frustules, if one considers the hundreds of siliceous frustules tightly packed into each fecal pellet. For example, individual measurements of Si content of fecal pellets produced by large copepods carried out near the Polar Front by Dagg et al. (2003) indicated the potential for daily ingestion and excretion of 1×10^4 to $>1 \times 10^6$ equivalent diatom cells in terms of Si amount.

4.3. Life stages: resting spores and winter forms

Diatom resting stages were more frequently observed in the HNLC waters west of Kerguelen and over the plateau than at station M1 and were only observed in centric species. The winter stage/resting spore formation is usually preferentially observed in centric diatoms and in the coastal environments possibly allowing cells that have sunk to the sediments to resurface upon a later mixing event (McQuoid and Hobson, 1996). At M4 and M3 a particular solitary stage of *Chaetoceros atlanticus*, with sigmoidal setae (which we hypothesize is a resting cell form) and, in lesser abundance, the spore form (*C. atlanticus f. bulbosum*) were dominant. On the plateau area, the abundance of the *C. atlanticus* complex was minor.

The plateau, which was the most Si-limited region at the end of summer Si/DIN ratios as low as 0.05-0.11), was dominated by the winter stage of *Eucampia antarctica* in the process of sinking out of the surface layer following a previous bloom, as they were more abundant in intermediate layer Bottle nets than in the surface Phytonets. Our results are consistent with observations reported for the Crozet diatom export study in a similar comparison of an Fe-fertilized plateau vs. an Fe-limited station further off in the open ocean (Salter et al., 2012). In this latter study the contribution

to diatom downward export flux of viable heavily silicified *E. antarctica* with well preserved winter stages was dominant on the plateau (up to 71% contribution) while the vegetative stage was almost entirely absent. As nitrate was non-limiting the authors suggested that low dissolved Fe and silicic acid concentrations at the end of the growth season were plausible triggers for the development of the winter stage and its subsequent sinking, which was tightly correlated to the enhanced C flux measured on the plateau (Salter et al., 2012). Winter forms of *E. antarctica* were also abundant on the sediment floor of the Kerguelen Plateau (Armand et al., 2008b), confirming the important role of this emblematic species to the C pump in Fe-fertilized areas in the wake of Southern Ocean island.

Eucampia antarctica co-occurred with *Odontella weissflogii*, which were likely sporulating, as resting cells and spores were present in the shallow Bottle net samples and much less abundant than *E. antarctica* at depth. Microscopic observations on board revealed healthy looking spores (packed with lipids), which, referring to observations by Kuwata et al. (1993) on *Chaetoceros pseudocurvisetus*, further confirms the recent sporulation and on-going sedimentation event.

The exploratory sporulation/germination experiments conducted at M2 strongly suggest that Si availability was the key trigger for spore formation, since the light treatment yielded 3 times less vegetative cells of *Odontella weissflogii* than the Si+light treatment (Table 5). Furthermore, the number of abnormal valves and general condition of germinated cells were a clear indication of Si limitation, while nitrate was still sufficient ($>21 \mu\text{M}$). In the sporulation experiment the light deprivation in low nutrient waters stimulated a 30 % increase in *O. weissflogii* resting stages, while *Eucampia antarctica* winter stages increased by a factor of 3 (Table 6), which could reflect different species-specific responses to environmental triggers.

Small *Thalassiosira* and *Chaetoceros* spores ($<20 \mu\text{m}$) were abundant in Niskin bottle samples below the mixed layer at M2 and M1 (Lafond et al., 2020) but were neither observed in Phytonets nor Bottle nets because of too large mesh sizes (35 and $20 \mu\text{m}$). Even though in small abundances, they however could contribute up to 40% of diatom C biomass at these sites below the mixed layer (Lafond et al., 2020) and are therefore potentially largely underestimated in the deep Bottle net casts. Our observations are congruent with previous reports of increased dominance of *Chaetoceros Hylaochaete* resting spores in trap samples (Rembauville et al., 2016) and of their dominance associated with *Eucampia antarctica* in sediments over the Kerguelen plateau (Armand et al., 2008b). As mentioned above, the formation of these spores could have been related to a viral infection (Pelusi et al, 2020).

4.4. Silicification degree and role in export

A schematic graph of diatom communities, Si:C stoichiometry and key processes both on and off-plateau is presented in Fig. 9 in order to summarize and bring together in one conceptual figure both surface and deep water data from this study and Lafond et al. (2020). Clear differences were observed between plateau and non-plateau waters for stoichiometric Si:C ratios in particulate matter based on diatom

carbon biomass, with the highest average Si:C_{diatoms} ratios estimated by Lafond et al. (2020) from Niskin bottles at non-plateau stations (2.7 ± 0.7) and the lowest on the plateau (0.6 ± 0.2). The other major result concerns the C and Si stocks in the deep compartment (above 125 m), which are both higher in the HNLC zone than on the plateau. Although resulting from stock evaluations from Niskin samples (Lafond et al, 2020) but referring to our previous studies (Mosseri et al, 2008; Lasbleiz et al, 2014) this illustrates the "High Production Low Export" character of the plateau waters as opposed to the "Low Production High Export" character of the HNLC zone according to the nomenclature of Henson *et al.* (2019). In a same way Rembauville et al (2015) had previously illustrated the "High Biomass Low Export" character of the plateau waters.

Particulate Σ BSi and C_{diatom} stock estimates for the intermediate layer (from bottle net samples) yield extremely high Si:C ratios (>180,000) which do not reflect on the silicification degree of cells but rather on the high detrital Si biomass content in this layer and loss of C during sinking. Nevertheless, microscopic observations confirmed the dominance of more heavily silicified species outside the Fe-fertilized plateau with a large dominance of the *Chaetoceros atlanticus* 'bulbosum' complex and *Fragilariopsis kerguelensis* at M4/M3 (Fig. 6). Frustule abundance was dominated by these two taxa, their elevated contribution to the downward Si flux. *F. kerguelensis* is known to be the dominant species in sediment and the main opal contributor of the summer Permanently Open Ocean Zone where it accounts for ~80% of the total diatom assemblage (Crosta et al., 2005) and its maximum occurrence is reported in 1-7°C waters (Jacques, 1983), which covers the temperature range measured during MOBYDICK (2-5°C). In our study region the contribution of *F. kerguelensis* in the sediment varies between 30 and 75%, while *Thalassiosira lentiginosa*, which was also abundant here, is the second most abundant taxon in Southern Ocean sediments with a reported range from 5-30% and has the same distribution pattern in the sediments than *F. kerguelensis* (Crosta et al., 2005; Shukla et al., 2016). This is consistent with our findings showing that *F. kerguelensis* is the dominant contributor to biomass in the deepest sample at M4 (Fig. 7), suggesting that it is the most efficient species at injecting C below the 2,000 m horizon. On the plateau (M2), the weakly silicified *Corethron inerme* was dominant in the surface layer, but the deep particle stock was also enriched with more heavily silicified species such as *Eucampia antarctica* and *F. kerguelensis* even though in lesser numbers than west of Kerguelen.

It should also be noted that that *F. kerguelensis* silicification degree, quantified with a silicification fluorescent probe (Lafond et al., 2020), was higher at M4/M3/M1 than at M2, reflecting the different ecological situations regarding Fe limitation. Hence, both taxonomic differences (mix of *Corethron* with *Eucampia* and *Fragilariopsis*) and lesser silicification degree of the dominant species can explain the lower Si/C_{diatom} ratios on the plateau. Finally, *Eucampia* and *Fragilariopsis* were the dominant contributors to the Si flux while *Corethron inerme* was the main contributing species to C export, in particular upon the last visit at M2 (Fig. 7), again showing differences in the relative contribution of diatom species to Si and C export.

suspended and sinking particles in the ocean's interior. The Bottle net allowed to carry out a detailed study of diatom taxonomy, C biomass, physiological state of cells, trophic behaviour and life cycles on depth-integrated concentrated material which could not have been obtained from discrete deep Niskin samples, in which particle concentration is much too low for such analysis. In particular, it allowed to identify various mortality modes at the end of the final summer bloom. *Fragilariopsis kerguelensis*, which was previously considered as a very resistant species against grazers (Hamm et al., 2003; Assmy et al., 2013; Quéguiner, 2013), has been shown here to be actively grazed by mesozooplankton with a lot of crunched frustules but also ingested by phaeodarian barely larger than the diatom cell length. High contents of crushed frustules debris observed in fecal pellets and minipellets also showed that this species is indeed palatable for various grazers of different sizes. The Bottle net also allowed to collect small-sized particles and to evidence that minipellets were the dominant fecal material in the water column at this stage of the season. Unfortunately, we could not estimate their contribution to the deep C stocks even though previous studies have already shown that it could be important.

The Bottle net could also help identify sporulation events linked to surface Si-limitation over the plateau and evidence an important parasitic infection of diatoms. We could however not conclude from our data as to whether the infected cells found below the mixed layer were the result of direct injection of biomass following cell death and subsequent sinking or if this was the result of a strong deep mixing event following a storm. There is still conflicting evidence on the fate of infected cells (lysis in the surface layer or deep layer injection), which needs to be investigated further. Much more emphasis will need to be placed on the end of bloom periods during field work in order to be able to progress on identifying processes leading to the demise of the blooms and to understand how parasites and viruses may alter species succession and the fate of primary produced C. We also want to stress that live observations on board are absolutely necessary in identifying different trophic behaviors such as infection by parasites that can be easily overlooked when examining fixed samples back at the ground-based laboratory.

Finally, future sampling strategies will need to incorporate the biogeochemical and taxonomic characteristics of all components of vertical particle flux in a more integrated manner, allowing the intensity of the biological carbon pump to be more precisely related to environmental conditions. This strategic development should prove to be crucial to provide elements for predicting the evolution of the biological carbon pump in these times of rapid climate change.

Acknowledgments

We thank B. Quéguiner, the PI of the MOBYDICK project, for providing us the opportunity to participate to this cruise, the chief scientist I. Obernosterer and the captain and crew of the R/V Marion Dufresne for their enthusiasm and support aboard during the MOBYDICK-THEMISTO cruise (doi:10.1BE00/1F00040G). This work was supported by the French oceanographic fleet ("Flotte océanographique française"), the French ANR ("Agence Nationale de la Recherche", AAPC 201B

program, MOBYDICK Project number: ANR-1B-CE01-001G), and the French Research program of INSH-CNRS LEFE/CYBER (“Les enveloppes fluides et l’environnement” – “Cycles biogéochimiques, environnement et ressources”). We thank Dr. D. Vaultot and I. Probert who gave us access to the Phenom-Pro at the Roscoff Biological Station. The authors wish also to thank Frédéric Le Moigne for constructive discussions on this paper.

Declaration of interests

The authors declare that they have no known competing financial interests or personal relationships that could have appeared to influence the work reported in this paper.

References

- Agusti, S., Gonzalez-Gordillo, J.I., Vaque, D., Estrada, M., Cerezo, M.I., Salazar, G., Gasol, J.M., Duarte, C.M., 2015. Ubiquitous healthy diatoms in the deep sea confirm deep carbon injection by the biological pump. *Nat Commun* 6, 7608.
- Agustí, S., Krause, J.W., Marquez, I.A., Wassmann, P., Kristiansen, S., Duarte, C.M., 2020. Arctic (Svalbard islands) active and exported diatom stocks and cell health status. *Biogeosciences* 17, 35-45.
- Allredge, A.L., Gotschalk, C.C., 1990. The Relative Contribution of Marine Snow of Different Origins to Biological Processes in Coastal Waters. *Cont Shelf Res* 10, 41-58.
- Allredge, A.L., Silver, M.W., 1988. Characteristics, Dynamics and Significance of Marine Snow. *Prog Oceanogr* 20, 41-82.
- Armand, L.K., Cornet-Barthaux, V., Mosseri, J., Quéguiner, B., 2008a. Late summer diatom biomass and community structure on and around the naturally iron-fertilised Kerguelen Plateau in the Southern Ocean. *Deep-Sea Research Part II-Topical Studies in Oceanography* 55, 653-676.
- Armand, L.K., Crosta, X., Queguiner, B., Mosseri, J., Garcia, N., 2008b. Diatoms preserved in surface sediments of the northeastern Kerguelen Plateau. *Deep-Sea Research Part II-Topical Studies in Oceanography* 55, 677-692.
- Armand, L.K., Zielinski, U., 2001. Diatom species of the genus *Rhizosolenia* from Southern Ocean sediments: Distribution and taxonomic notes. *Diatom Res* 16, 259-294.
- Assmy, P., Henjes, J., Klaas, C., Smetacek, V., 2007. Mechanisms determining species dominance in a phytoplankton bloom induced by the iron fertilization experiment EisenEx in the Southern Ocean. *Deep-Sea Res Pt II* 54, 340-362.
- Assmy, P., Smetacek, V., Montresor, M., Klaas, C., Henjes, J., Strass, V.H., Arrieta, J.M., Bathmann, U., Berg, G.M., Breitbarth, E., Cisewski, B., Friedrichs, L., Fuchs, N., Herndl, G.J., Jansen, S., Kragefsky, S., Latasa, M., Peeken, I., Rottgers, R., Scharek, R., Schuller, S.E., Steigenberger, S., Webb, A., Wolf-Gladrow, D., 2013. Thick-shelled, grazer-protected diatoms decouple ocean carbon and silicon cycles in

1130 the iron-limited Antarctic Circumpolar Current. Proceedings of the National Academy
1131 of Sciences of the United States of America 110, 20633-20638.

1132 Biard, T., Krause, J.W., Stukel, M.R., Ohman, M.D., 2018. The Significance of giant
1133 Phaeodarians (Rhizaria) to Biogenic Silica Export in the California Current
1134 Ecosystem. Global Biogeochemical Cycles.

1135 Blain S., Quéguiner B., Trull T.W., 2008. The natural iron fertilization experiment
1136 KEOPS (KErguelen Ocean and Plateau compared Study): An overview. Deep Sea
1137 Research Part II: Topical Studies in Oceanography, 55 (5-7), 559-565.

1138 Blain, S., Rembauville, M., Crispi, O., Obernosterer, I., 2020. Synchronized
1139 autonomous sampling reveals coupled pulses of biomass and export of
1140 morphologically different diatoms in the Southern Ocean. Limnology and
1141 Oceanography.

1142 Brzezinski M.A., 1985. The Si:C:N ratio of marine diatoms: interspecific variability and
1143 the effect of some environmental variables. Journal of Phycology, 21, 347-357.

1144

1145 Close, H.G., Shah, S.R., Ingalls, A.E., Diefendorf, A.F., Brodie, E.L., Hansman, R.L.,
1146 Freeman, K.H., Aluwihare, L.I., Pearson, A., 2013. Export of submicron particulate
1147 organic matter to mesopelagic depth in an oligotrophic gyre. Proceedings of the
1148 National Academy of Sciences 110, 12565-12570.

1149 Cornet-Barthaux, V., Armand, L., Queguiner, B., 2007. Biovolume and biomass
1150 estimates of key diatoms in the Southern Ocean. Aquat Microb Ecol 48, 295-308.

1151 Crosta, X., Romero, O., Armand, L.K., Pichon, J.J., 2005. The biogeography of major
1152 diatom taxa in Southern Ocean sediments: 2. Open ocean related species.
1153 Palaeogeogr Palaeocl 223, 66-92.

1154 Dall'Olmo, G., Mork, K.A., 2014. Carbon export by small particles in the Norwegian
1155 Sea. Geophys Res Lett 41, 2921-2927.

1156 DiTullio, G., Grebmeier, J., Arrigo, K., Lizotte, M., Robinson, D., Leventer, A., Barry,
1157 J., VanWoert, M., Dunbar, R., 2000. Rapid and early export of *Phaeocystis antarctica*
1158 blooms in the Ross Sea, Antarctica. Nature 404, 595-598.

1159 Durkin, C.A., Estapa, M.L., Buesseler, K.O., 2015. Observations of carbon export by
1160 small sinking particles in the upper mesopelagic. Mar Chem 175, 72-81.

1161 Durkin, C.A., Koester, J.A., Bender, S.J., Armbrust, E.V., 2016. The evolution of
1162 silicon transporters in diatoms. J Phycol 52, 716-731.

1163 Ellegaard, M., Ribeiro, S., 2018. The long-term persistence of phytoplankton resting
1164 stages in aquatic 'seed banks'. Biological Reviews 93, 166-183.

1165 Eppley, R.W., Reid, F.M.H., Strickland, J.D.H., 1970. The ecology of the plankton off
1166 La Jolla, California, in the period April through September, 1967. III. Estimates of
1167 phytoplankton crop, size, growth rate, and primary production. Bull. Scripps Inst.
1168 Oceanogr. 17, 33--42.

1169 Fryxell, G.A., Prasad, A.K.S.K., 1990. *Eucampia antarctica* var. *recta* (Mangin) stat.
1170 nov. (Biddulphiaceae, Bacillariophyceae): life stages at the Weddell Sea ice edge.
1171 Phycologia 29, 27-38.

1172 Gardner, W.D., Chung, S.P., Richardson, M.J., Walsh, I.D., 1995. The oceanic
1173 mixed-layer pump. *Deep Sea Research Part II: Topical Studies in Oceanography* 42,
1174 757-775.

1175 Giering, S.L., Sanders, R., Lampitt, R.S., Anderson, T.R., Tamburini, C., Boutrif, M.,
1176 Zubkov, M.V., Marsay, C.M., Henson, S.A., Saw, K., Cook, K., Mayor, D.J., 2014.
1177 Reconciliation of the carbon budget in the ocean's twilight zone. *Nature* 507, 480-
1178 483.

1179 Gonzalez, H.E., 1992. Distribution and abundance of minipellets around the Antarctic
1180 peninsula. Implications for protistan feeding behaviour. *Mar Ecol Prog Ser* 90, 223-
1181 223.

1182 Gowing, M.M., 1986. Trophic biology of phaeodarian radiolarians and flux of living
1183 radiolarians in the upper 2000 m of the North Pacific central gyre. *Deep Sea*
1184 *Research Part A. Oceanographic Research Papers* 33, 655-674.

1185 Gowing, M.M., 1989. Abundance and feeding ecology of Antarctic phaeodarian
1186 radiolarians. *Mar Biol* 103, 107-118.

1187 Gowing, M.M., Silver, M.W., 1985. Minipellets: a new and abundant size class of
1188 marine fecal pellets. *J Mar Res* 43, 395-418.

1189 Greenspan, P., 1985. Nile red: a selective fluorescent stain for intracellular lipid
1190 droplets. *The Journal of Cell Biology* 100, 965-973.

1191 Gutiérrez, M.H., Jara, A.M., Pantoja, S., 2016. Fungal parasites infect marine
1192 diatoms in the upwelling ecosystem of the Humboldt current system off central Chile.
1193 *Environmental Microbiology* 18, 1646-1653.

1194 Gutierrez-Rodriguez, A., Stukel, M.R., dos Santos, A.L., Biard, T., Scharek, R.,
1195 Vaulot, D., Landry, M.R., Not, F., 2019. High contribution of Rhizaria (Radiolaria) to
1196 vertical export in the California Current Ecosystem revealed by DNA metabarcoding.
1197 *The ISME journal* 13, 964-976.

1198 Hamm, C.E., Merkel, R., Springer, O., Jurkojc, P., Maier, C., Prechtel, K., Smetacek,
1199 V., 2003. Architecture and material properties of diatom shells provide effective
1200 mechanical protection. *Nature* 421, 841-843.

1201 Henson, S.A., Sanders, R., Madsen, E., Morris, P.J., Le Moigne, F., Quartly, G.D.,
1202 2011. A reduced estimate of the strength of the ocean's biological carbon pump.
1203 *Geophys Res Lett* 38.

1204 Henson S., Le Moigne F., Giering S., 2019. Drivers of carbon export efficiency in the
1205 global ocean. *Global Biogeochemical Cycles*, 33 (7), 891-903.

1206 Howard, A.G., Coxhead, A.J., Potter, I.A., Watt, A.P., 1986. Determination of
1207 dissolved aluminium by the micelle-enhanced fluorescence of its lumogallion
1208 complex. *Analyst* 111, 1379-1382.

1209 Landry, M.R., Selph, K.E., Brown, S.L., Abbott, M.R., Measures, C.I., Vink, S., Allen,
1210 C.B., Calbet, A., Christensen, S., Nolla, H., 2002. Seasonal dynamics of
1211 phytoplankton in the Antarctic Polar Front region at 170°W. *Deep Sea Research Part*
1212 *II: Topical Studies in Oceanography* 49, 1843-1865.

1213 Ikenoue, T., Kimoto, K., Okazaki, Y., Sato, M., Honda, M.C., Takahashi, K., Harada,
1214 N., Fujiki, T., 2019. Phaeodaria: An Important Carrier of Particulate Organic Carbon

1215 in the Mesopelagic Twilight Zone of the North Pacific Ocean. *Global Biogeochemical*
1216 *Cycles* 33, 1146-1160.

1217 Iversen, M.H., Lampitt, R.S., 2020. Size does not matter after all: No evidence for a
1218 size-sinking relationship for marine snow. *Prog Oceanogr* 189.

1219 Jacques G., 1983. Some ecophysiological aspects of the Antarctic phytoplankton.
1220 *Polar Biology*, 2, 27-33.

1221

1222 Kaczmarska, I., Pouličková, A., Sato, S., Edlund, M.B., Idei, M., Watanabe, T., Mann,
1223 D.G., 2013. Proposals for a terminology for diatom sexual reproduction, auxospores
1224 and resting stages. *Diatom Res* 28, 263-294.

1225 Kemp, A.E.S., Pike, J., Pearce, R.B., Lange, C.B., 2000. The “Fall dump”- a new
1226 perspective on the role of a “shade flora” in the annual cycle of diatom production
1227 and export flux. *Deep Sea Research Part II: Topical Studies in Oceanography* 47,
1228 2129-2154.

1229 Klaas C., Archer D.E., 2002. Association of sinking organic matter with various types
1230 of mineral ballast in the deep sea: Implications for the rain ratio. *Global*
1231 *Biogeochemical Cycles*, 16 (4), 63-61 - 63-14.

1232 Kranzler, C.F., Krause, J.W., Brzezinski, M.A., Edwards, B.R., Biggs, W.P.,
1233 Maniscalco, M., McCrow, J.P., Van Mooy, B.A., Bidle, K.D., Allen, A.E., 2019. Silicon
1234 limitation facilitates virus infection and mortality of marine diatoms. *Nature*
1235 *microbiology*, 1-8.

1236 Laber, C.P., Hunter, J.E., Carvalho, F., Collins, J.R., Hunter, E.J., Schieler, B.M.,
1237 Boss, E., More, K., Frada, M., Thamatrakoln, K., Brown, C.M., Haramaty, L.,
1238 Ossolinski, J., Fredricks, H., Nissimov, J.I., Vandzura, R., Sheyn, U., Lehahn, Y.,
1239 Chant, R.J., Martins, A.M., Coolen, M.J.L., Vardi, A., DiTullio, G.R., Van Mooy,
1240 B.A.S., Bidle, K.D., 2018. Coccolithovirus facilitation of carbon export in the North
1241 Atlantic. *Nat Microbiol* 3, 537-547.

1242 Lafond, A., Leblanc, K., Legras, J., Cornet, V., Quéguiner, B., 2020. The structure of
1243 diatom communities constrains biogeochemical properties in surface waters of the
1244 Southern Ocean (Kerguelen Plateau). *J Marine Syst*, 103458.

1245 Lam, P.J., Marchal, O., 2015. Insights into particle cycling from thorium and particle
1246 data. *Annual review of marine science* 7, 159-184.

1247 Lampitt, R.S., Salter, I., Johns, D., 2009. Radiolaria: Major exporters of organic
1248 carbon to the deep ocean. *Global Biogeochemical Cycles* 23, GB1010.

1249 Lasbleiz, M., Leblanc, K., Armand, L.K., Christaki, U., Georges, C., Obernosterer, I.,
1250 Quéguiner, B., King, G., 2016. Composition of diatom communities and their
1251 contribution to plankton biomass in the naturally iron-fertilized region of Kerguelen in
1252 the Southern Ocean. *FEMS microbiology ecology* 92, 653--676.

1253 Lasbleiz, M., Leblanc, K., Blain, S., Ras, J., Cornet-Barthaux, V., Hélias Nunige, S.,
1254 Quéguiner, B., 2014. Pigments, elemental composition (C, N, P, and Si), and
1255 stoichiometry of particulate matter in the naturally iron fertilized region of Kerguelen
1256 in the Southern Ocean. *Biogeosciences* 11, 5931-5955.

1257 Laurenceau-Cornec, E.C., Trull, T.W., Davies, D.M., Bray, S.G., Doran, J., Planchon,
1258 F., Carlotti, F., Jouandet, M.P., Cavagna, A.J., Waite, A.M., Blain, S., 2015. The

1259 relative importance of phytoplankton aggregates and zooplankton fecal pellets to
 1260 carbon export: insights from free-drifting sediment trap deployments in naturally iron-
 1261 fertilised waters near the Kerguelen Plateau. *Biogeosciences* 12, 1007-1027.

1262 Laurenceau-Cornec, E.C., Le Moigne, F.A., Gallinari, M., Moriceau, B., Toullec, J.,
 1263 Iversen, M.H., Engel, A., De La Rocha, C.L., 2020. New guidelines for the application
 1264 of Stokes' models to the sinking velocity of marine aggregates. *Limnology and*
 1265 *Oceanography* 65, 1264-1285.

1266 Laws, E.A., Landry, M.R., Barber, R.T., Campbell, L., Dickson, M.-L., Marra, J., 2000.
 1267 Carbon cycling in primary production bottle incubations: inferences from grazing
 1268 experiments and photosynthetic studies using and in the Arabian Sea. *Deep Sea*
 1269 *Research Part II: Topical Studies in Oceanography* 47, 1339-1352.

1270 Le Moigne, F.A.C., 2019. Pathways of Organic Carbon Downward Transport by the
 1271 Oceanic Biological Carbon Pump. *Frontiers in Marine Science* 6.

1272 Leblanc, K., Queguiner, B., Diaz, F., Cornet, V., Michel-Rodriguez, M., Durrieu de
 1273 Madron, X., Bowler, C., Malviya, S., Thyssen, M., Gregori, G., Rembauville, M.,
 1274 Grosso, O., Poulain, J., de Vargas, C., Pujo-Pay, M., Conan, P., 2018.
 1275 Nanoplanktonic diatoms are globally overlooked but play a role in spring blooms and
 1276 carbon export. *Nat Commun* 9, 953.

1277 Lundsgaard, C., 1994. Use of high viscosity medium in studies of aggregates,
 1278 Sediment Trap Studies in the Nordic Countries. *Symposium Proc., Mar. Biol. Lab.,*
 1279 *Helsingør, Denmark*, pp. 141-152.

1280 McDonnell, A.M., Lam, P.J., Lamborg, C.H., Buesseler, K.O., Sanders, R., Riley,
 1281 J.S., Marsay, C., Smith, H.E., Sargent, E.C., Lampitt, R.S., 2015. The oceanographic
 1282 toolbox for the collection of sinking and suspended marine particles. *Prog Oceanogr*
 1283 133, 17-31.

1284 McQuoid, M.R., Hobson, L.A., 1996. Diatom Resting Stages. *J Phycol* 32, 889-902.

1285 Mosseri, J., Quéguiner, B., Armand, L., Cornet-Barthaux, V., 2008. Impact of iron on
 1286 silicon utilization by diatoms in the Southern Ocean: A case study of Si/N cycle
 1287 decoupling in a naturally iron-enriched area. *Deep Sea Research Part II: Topical*
 1288 *Studies in Oceanography* 55, 801-819.

1289 Nakamura, Y., Suzuki, N., 2015. Phaeodaria: diverse marine cercozoans of world-
 1290 wide distribution, *Marine Protists*. Springer, pp. 223-249.

1291 Omand, M.M., D'Asaro, E.A., Lee, C.M., Perry, M.J., Briggs, N., Cetinić, I.,
 1292 Mahadevan, A., 2015. Eddy-driven subduction exports particulate organic carbon
 1293 from the spring bloom. *Science* 348, 222-225.

1294 Park, Y.H., Durand, I., Kestenare, E., Rougier, G., Zhou, M., d'Ovidio, F., Cotté, C.,
 1295 Lee, J.H., 2014. Polar Front around the Kerguelen Islands: An up-to-date
 1296 determination and associated circulation of surface/subsurface waters. *Journal of*
 1297 *Geophysical Research: Oceans* 119, 6575-6592.

1298 Pauthenet, E., Roquet, F., Madec, G., Guinet, C., Hindell, M., McMahon, C.R.,
 1299 Harcourt, R., Nerini, D., 2018. Seasonal Meandering of the Polar Front Upstream of
 1300 the Kerguelen Plateau. *Geophys Res Lett* 45, 9774-9781.

1301 Pelusi, A., De Luca, P., Manfellotto, F., Thamatrakoln, K., Bidle, K.D., Montresor, M.,
1302 2020. Virus-induced spore formation as a defense mechanism in marine diatoms.
1303 *New Phytol.*

1304 Priddle, J., Fryxell, G., 1985. Handbook of the common plankton diatoms of the
1305 Southern Ocean. British Antarctic Survey.

1306 Puigcorbé V., Masqué P., Le Moigne F.A.C., 2020. Global database of ratios of
1307 particulate organic carbon to thorium-234 in the ocean: improving estimates of the
1308 biological carbon pump. *Earth System Science Data*, 12 (2), 1267-1285.

1309 Quéguiner, B., 2013. Iron fertilization and the structure of planktonic communities in
1310 high nutrient regions of the Southern Ocean. *Deep Sea Research Part II: Topical*
1311 *Studies in Oceanography* 90, 43-54.

1312 Ragueneau, O., Savoye, N., Del Amo, Y., Cotten, J., Tardiveau, B., Leynaert, A.,
1313 2005. A new method for the measurement of biogenic silica in suspended matter of
1314 coastal waters: using Si:Al ratios to correct for the mineral interference. *Cont Shelf*
1315 *Res* 25, 697-710.

1316 Rembauville, M., Blain, S., Armand, L., Quéguiner, B., Salter, I., 2015. Export fluxes
1317 in a naturally iron-fertilized area of the Southern Ocean – Part 2: Importance of
1318 diatom resting spores and faecal pellets for export. *Biogeosciences* 12, 3171-3195.

1319 Rembauville, M., Manno, C., Tarling, G.A., Blain, S., Salter, I., 2016. Strong
1320 contribution of diatom resting spores to deep-sea carbon transfer in naturally iron-
1321 fertilized waters downstream of South Georgia. *Deep Sea Research Part I:*
1322 *Oceanographic Research Papers* 115, 22-35.

1323 Riaux-Gobin, C., Hargraves, P.E., Neveux, J., Oriol, L., Vétion, G., 1997. Microphyte
1324 pigments and resting spores at the water-sediment interface in the Subantarctic deep
1325 sea (Indian sector of the Southern Ocean). *Deep Sea Research Part II: Topical*
1326 *Studies in Oceanography* 44, 1033-1051.

1327 Riaux-Gobin, C., Fontugne, M., Jensen, K.G., Bentaleb, I., Cauwet, G., Chrétiennot-
1328 Dinet, M.J., Poisson, A., 2006. Surficial deep-sea sediments across the polar frontal
1329 system (Southern Ocean, Indian sector): Particulate carbon content and microphyte
1330 signatures. *Mar Geol* 230, 147-159.

1331 Richardson, T.L., Jackson, G.A., 2007. Small phytoplankton and carbon export from
1332 the surface ocean. *Science* 315, 838-840.

1333 Riemann, F., 1989. Gelatinous phytoplankton detritus aggregates on the Atlantic
1334 deep-sea bed. *Mar Biol* 100, 533-539.

1335 Rigual-Hernández, A.S., Trull, T.W., Bray, S.G., Armand, L.K., 2016. The fate of
1336 diatom valves in the Subantarctic and Polar Frontal Zones of the Southern Ocean:
1337 Sediment trap versus surface sediment assemblages. *Palaeogeography,*
1338 *Palaeoclimatology, Palaeoecology* 457, 129-143.

1339 Rigual-Hernández, A.S., Trull, T.W., Bray, S.G., Closset, I., Armand, L.K., 2015.
1340 Seasonal dynamics in diatom and particulate export fluxes to the deep sea in the
1341 Australian sector of the southern Antarctic Zone. *J Marine Syst* 142, 62-74.

1342 Riley, J., Sanders, R., Marsay, C., Le Moigne, F.A., Achterberg, E.P., Poulton, A.J.,
 1343 2012. The relative contribution of fast and slow sinking particles to ocean carbon
 1344 export. *Global Biogeochemical Cycles* 26.

1345 Romero, O.E., Fischer, G., 2017. Shift in the species composition of the diatom
 1346 community in the eutrophic Mauritanian coastal upwelling: Results from a multi-year
 1347 sediment trap experiment (2003–2010). *Prog Oceanogr* 159, 31-44.

1348 Salter, I., Kemp, A.E.S., Moore, C.M., Lampitt, R.S., Wolff, G.A., Holtvoeth, J., 2012.
 1349 Diatom resting spore ecology drives enhanced carbon export from a naturally iron-
 1350 fertilized bloom in the Southern Ocean. *Global Biogeochemical Cycles* 26, n/a-n/a.

1351 Salter, I., Lampitt, R.S., Sanders, R., Poulton, A., Kemp, A.E.S., Boorman, B., Saw,
 1352 K., Pearce, R., 2007. Estimating carbon, silica and diatom export from a naturally
 1353 fertilised phytoplankton bloom in the Southern Ocean using PELAGRA: A novel
 1354 drifting sediment trap. *Deep Sea Research Part II: Topical Studies in Oceanography*
 1355 54, 2233-2259.

1356 Sassenhagen, I., Irion, S., Jardillier, L., Moreira, D., Christaki, U., 2020. Protist
 1357 Interactions and Community Structure During Early Autumn in the Kerguelen Region
 1358 (Southern Ocean). *Protist* 171, 125709.

1359 Scholz, B., Guillou, L., Marano, A.V., Neuhauser, S., Sullivan, B.K., Karsten, U.,
 1360 Kupper, F.C., Gleason, F.H., 2016. Zoospore parasites infecting marine diatoms - A
 1361 black box that needs to be opened. *Fungal Ecol* 19, 59-76.

1362 Scott, F.J., Marchant, H.J., 2005. Antarctic marine protists. Australian Biological
 1363 Resources Study Canberra.

1364 Shukla, S.K., Crespín, J., Crosta, X., 2016. *Thalassiosira lentiginosa* size variation
 1365 and associated biogenic silica burial in the Southern Ocean over the last 42 kyrs.
 1366 *Marine Micropaleontology* 127, 74-85.

1367 Smayda, T.J., 1978. From phytoplankton to biomass. 6. Phytoplankton manual.

1368 Smith, H.E., 2014. The contribution of mineralising phytoplankton to the biological
 1369 carbon pump in high latitudes. University of Southampton.

1370 Stemmann, L., Jackson, G.A., Gorsky, G., 2004. A vertical model of particle size
 1371 distributions and fluxes in the midwater column that includes biological and physical
 1372 processes—Part II: application to a three year survey in the NW Mediterranean Sea.
 1373 *Deep Sea Research Part I: Oceanographic Research Papers* 51, 885-908.

1374 Stukel, M.R., Biard, T., Krause, J., Ohman, M.D., 2018. Large Phaeodaria in the
 1375 twilight zone: Their role in the carbon cycle. *Limnology and Oceanography* 63, 2579-
 1376 2594.

1377 Suttle, C.A., 2007. Marine viruses major players in the global ecosystem. *Nature*
 1378 *Reviews Microbiology*, 5 (10), 801-812.

1379 Turner, J.T., 2002. Zooplankton fecal pellets, marine snow and sinking phytoplankton
 1380 blooms. *Aquat Microb Ecol* 27, 57-102.

1381 Veldhuis, M., Kraay, G., Timmermans, K., 2001. Cell death in phytoplankton:
 1382 correlation between changes in membrane permeability, photosynthetic activity,
 1383 pigmentation and growth. *Eur J Phycol* 36, 167-177.

1384 Waite, A.M., Safi, K.A., Hall, J.A., Nodder, S.D., 2000. Mass sedimentation of
1385 picoplankton embedded in organic aggregates. *Limnology and Oceanography* 45,
1386 87-97.

1387

1388

1389